POLITECNICO DI TORINO

Department of Control and Computer Engineering (DAUIN)

Master of Science in Mechatronic Engineering

Master Degree Thesis

Model Predictive Control of an Inertial Sea Wave Energy Converter

Supervisors:

Prof. Massimo Canale
Prof. Vito Cerone
Prof. Diego Regruto Tomalino

Author:

Yuri Evangelista

April 2019

Abstract

This thesis aims to design a controller for the *Inertial Sea Wave Energy Converter* (ISWEC) system based on the *Model Predictive Control* (MPC) technique with the goal of maximizing the produced electric power by converting the energy owned by the sea motions into electric energy. The energy conversion takes place through the *Power Take-Off* (PTO) unit, which is the object of the system to be controlled. The design stage of the controller aims to find a suitable tradeoff among different requirements such as energy production, command effort and PTO shaft speed limitation. Constraints of the ISWEC system such as the feasible bounds of the actuator are taken into account explicitly in the problem . A linear model of the ISWEC system is employed for implementing the MPC optimization problem as a *quadratic programme* (QP), to obtain a fast online implementation on the processor control unit present in the considered ISWEC system by means of an efficient solver. Numerical simulations of a detailed ISWEC nonlinear model have been performed to test the effectiveness of the designed controller. The obtained results are shown and discussed.

Contents

List of Figures

List of Tables

Chapter 1

Introduction

Ocean wave energy is one of the most promising renewable energy source and realizes a significant contribution in the world energy mix, as discussed in [1]. The ocean owns different energy sources such as wave motion, current tide, salinity gradient, temperature differential and offshore wind. The wave motion is the ocean energy source topic of this thesis work, as it realizes the excitation input of the considered system to control. Moreover, wave energy is one of the densest since it allows yearly extraction of an average power density up to 80 kW per meter of shoreline. Energy harvesting from wave motion has been topic of many research activities in the world since the oil crisis in the seventies. In the last twenty years the main purpose of such activities has been developing suitable devices capable to effectively produce energy facing issues such as reliability and efficiency, in order to achieve effective performance in terms of energy production cost. Nowadays different *Wave Energy Converter* (WEC) devices have been developed and tested in the sea with promising results, as reported in [2] and [3] where it is presented a thorough review of existing WEC systems.

In this thesis work the *Inertial Sea Wave Energy Converter* (ISWEC) developed in *Politecnico di Torino* is considered. A picture of the ISWEC in Pantelleria sea is reported in figure 1.1.

Figure 1.1: ISWEC system in Pantelleria

The ISWEC project started in 2006 at Politecnico di Torino and involved several modelling and experimental activities at different scale levels. In August 2015, a full scale 100 kW prototype has been constructed and located near the shore of Pantelleria island (Sicily, Italy), which is one of the most effective energy sites in the Mediterranean sea.

The ISWEC system consists of a floating device composed of a hull which hosts inside a gyroscope system whose motion is induced by the pitching oscillations of the hull floating on the sea surface. Energy extraction is obtained by damping the gyroscope precession motion through an electrical Power Take-Off (PTO) unit, which is implemented by an electric motor able to exert a torque intended for damping such a motion.
The adoption of a gyroscopic systems for energy production in sea wave energy context has been proposed first by Salter in Scotland [4], and more recently by Oceantec in Spain [5] and by the Tottori University in Japan [6]. These devices are related to ocean applications, but it has been proven that gyroscope motion exploitation is more effective for waves that are short and frequent, typical of the Mediterranean sea [7].

As already mentioned the energy harvesting is accomplished by damping the precession motion of the gyroscope by imposing a suitable torque to the PTO shaft. The damping action is computed by a suitable automatic control strategy, which in this thesis work it is based on the MPC technique. Different control strategies have been already applied to ISWEC system, as for example a quite effective PD controller has been employed to compute the PTO command torque, as discussed in [8]. Other control strategies have been investigated such as an LQR control strategy, discussed in [9] and an unconstrained Model Predictive Control, discussed in [10].

In this thesis work an original MPC control problem formulation is addressed for achieving different control requirements of the ISWEC system. The proposed MPC controller results to be a suitable technique for the ISWEC system as it allows to handle efficiently different requirements by tuning a customized quadratic cost function, which allows to find an optimal tradeoff among the different requirements such as energy production, command effort and PTO shaft speed limitation. In addition the MPC controller proposed in this thesis allows to take into account constraints of the system explicitly in the control problem, differently from [10], allowing thus the system to work closer to its limits leading therefore to an improved overall performance.

Thesis Structure

This thesis is organized in five chapters, including the current chapter 1, which introduces the context in which the thesis work is placed and the ISWEC system to be controlled.

Chapter 2 describes the **ISWEC system**. In particular it is discussed its structure and its main components relevant for understanding and addressing the control problem. Afterwards, the ISWEC dynamics are introduced discussing the dynamic equations and deriving their linearized version used for control purposes in the next chapters. Moreover, system constraints are presented and discussed. Eventually, the power extraction principle and the control requirements are presented.

Chapter 3 addresses the **MPC control problem** for the ISWEC system. The chapter opens introducing the MPC theory and its main aspects, defining thus all the key words present in this thesis work. Then, three different versions of MPC controller are designed and discussed. The first MPC controller designed is the most relevant one, as the successive versions provide some improvements relying on this version. The second developed MPC controller is referred to as *"Augmented MPC"* and consists of an upgraded version of the previously designed MPC using an augmented model to account for the wave contribution in the dynamics. The last developed MPC controller is referred to as *"MPC with Known Disturbance"*, which is characterized by the adoption of a more sophisticated prediction model which allows to better foresee the future dynamics of the system.
All the three developed controllers are addressed according to the following structure. First the control system architecture is presented and explained. Then, the control problem is developed, first from a theoretical point of view and then from the implementation point of view, discussing the tuning of the MPC controller parameters and the used software tools. Finally, simulations results of the detailed nonlinear ISWEC model are presented, showing the effectiveness of the designed MPC controller. The shown results are discussed and compared with past results provided by the previous ISWEC controller, which consists of a PD controller.

Chapter 4 investigates energy harvesting by using LQR control technique. The chapter introduces the main LQR theory concepts, then discusses the controller design, the implementation and the obtained results. LQR performances investigation results to be interesting as it consists in a static state-feedback control law, whose implementation results thus to be very effective from a computational point of view, that may therefore lead to adoption of less expensive processor platforms for its implementation.

Chapter 5 summarizes the conclusions obtained from the thesis work and proposes further possible developments.

Chapter 2

ISWEC System

The *Inertial Sea Wave Energy Converter* (*ISWEC*) is a system whose purpose is harvesting electric energy by converting the energy owned by the sea waves motion into electric energy. The following sections describe the ISWEC system and its main components relevant for understanding and addressing the control problem, as well as and its working principle and the dynamic equations which describe its behaviour. Moreover the linearized equations are derived, required for the control purposes.

2.1 System Description

The ISWEC consists of a hull floating on the sea surface which hosts in the inner environment different elements intended for producing and harvesting electrical energy. The hull inner environment is sealed such that the contained elements are safe from the outer environment, which could result otherwise dangerous. The main units hosted in the inner environment of the hull are the gyroscope system, which implements a spinning flywheel, and the *Power Take-Off* unit, which is the element intended for producing electric power. The ISWEC hull and the layout configuration of its main elements are shown in figure 2.1. The figure also show the reference frame XYZ of the gyroscope system fixed with the hull. The axes X-axis, Y-axis and Z-axis can be equivalently referred to as ε-axis, δ-axis and φ-axis respectively.

The parameters characterizing the ISWEC geometry and mass are reported table 2.1.

Table 2.1: ISWEC Parameters

Parameter	**Value**
Total Mass (of which sand ballast)	316 ton (200 ton)
Floater length	15 m
Floater width	8 m
Floater height	5 m

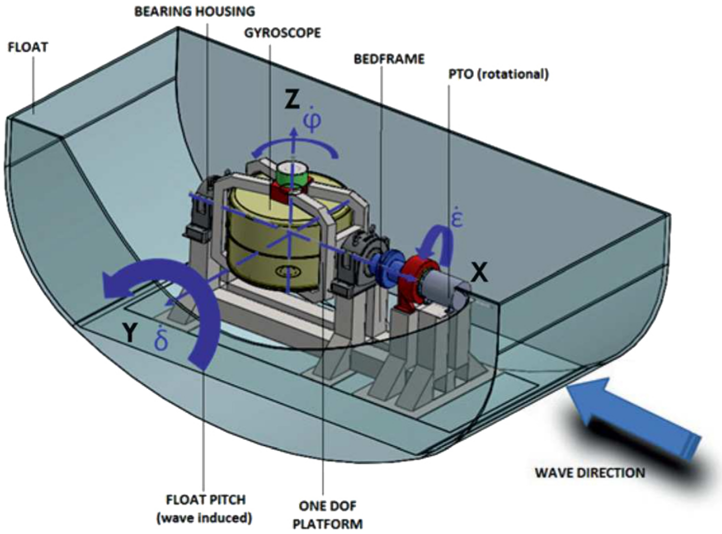

Figure 2.1: ISWEC System Components Layout

The gyroscope system is composed of a spinning flywheel which is enclosed in a case kept at low pressure for minimizing the drag resistance on the flywheel during the rotational motion. An electric motor is responsible for spinning the flywheel about the Z-axis. The flywheel case is mounted on a structure which allows the rotation about the X-axis. The physical phenomenon known as *gyroscopic effect* is responsible for rotating the spinning flywheel about the X-axis. More in details, as the gyroscope structure is rigidly connected to the hull floor, whenever the hull undergoes a rotation about the Y-axis due to the excitation of the incoming wave, then the spinning flywheel of the gyroscope system undergoes the same pitch motion, and therefore an induced torque occurs on the spinning flywheel given by *gyroscopic effect law* which induces the flywheel to rotate about the X-axis. This phenomenon is also known as *precession*, and the induced rotational motion is consequently known as *precession motion*.

The energy production takes place by exploiting *precession* phenomenon. In particular the energy extraction is obtained by damping the gyroscope precession motion through the Power Take-Off (PTO) unit. The PTO is implemented by an electric motor able to impose a suitable torque T_ε intended for damping such a precession motion. The gyroscope shaft about which the precession motion takes place is mechanically connected to the PTO shaft, and therefore the imposed torque by the PTO is able to damp the precession motion of the gyroscope system.

The ISWEC system in scale 1:1 working in Pantelleria implementes two gyroscope systems and consequently two PTO units. Such a system can be modelled as a system which implements only one gyroscope system connected to a single *equivalent* PTO unit. The equivalent PTO unit is characterized by the parameters reported in table 2.2.

Table 2.2: Equivalent PTO Parameters

Parameter	**Value**
Rated Power	250 kW
Rated Torque	100 kNm
Rated Speed	25 rpm

2.2 System Dynamics

The dynamics characterizing the ISWEC system can be classified into *external dynamics* and *internal dynamics*. External dynamics relate to the hull degrees of freedom and the forces exerted by the wave on the hull, taking into account thus hydrodynamic effects. Internal dynamics relate instead to the gyroscope system and are characterized by the mechanics of the flywheel taking into account the gyroscopic effect.
Internal dynamics and external dynamics are coupled, thus one affects the other and vice-versa.

The introduced dynamics can be modelled by writing suitable differential equations based on Newton torque equilibrium approach. As far as the *internal dynamics* are concerned, following this approach the resulting dynamic equations with respect to the reference frame XYZ presented in figure 2.1 are the following [14].

$$\begin{aligned} T_\varepsilon(t) &= I_g\,\ddot{\varepsilon}(t) + J_g\,\dot{\varphi}(t)\,\dot{\delta}(t)\cos\big(\varepsilon(t)\big) \\ T_\delta(t) &= I_g\,\ddot{\delta}(t) - J_g\,\dot{\varphi}(t)\,\dot{\varepsilon}(t)\cos\big(\varepsilon(t)\big) \\ T_\varphi(t) &= I_g\,\ddot{\delta}(t)\cos\big(\varepsilon(t)\big) - J_g\,\dot{\varepsilon}(t)\,\dot{\delta}(t) \end{aligned}$$

The variables $T_\varepsilon(t)$, $T_\delta(t)$ and $T_\varphi(t)$ represent the external torque exerted on the gyroscopic system respectively about X-axis, Y-axis and Z-axis. I_g is the total moment of inertia of the gyroscope system with respect to the ε-axis (or equivalently to the δ-axis due to the symmetry of the disc shape of the flywheel). J_g is the gyroscope axis-symmetric moment of inertia and $\dot{\varphi}(t)$ is the flywheel spinning speed. $\dot{\varepsilon}(t)$ is the precession angular velocity and $\dot{\delta}(t)$ is the hull pitching speed, whereas $\ddot{\varepsilon}(t)$ and $\ddot{\delta}(t)$ are respectively their angular acceleration.

As far as the *external dynamics* are concerned it is worth to notice that the ISWEC is self-orientating with respect to the incoming wave, thus the device interaction with waves can be casted to a planar problem in the plane defined by the vertical Z-axis and the bow-stern direction of the hull.
Therefore the external dynamics can be expressed through only one degree of freedom which represent the ISWEC pitch motion about the δ-axis.

The dynamic equation describing the ISWEC pitch dynamic is defined as [15]

$$\tau_w(t) = (I_h + \mu_\infty)\ddot{\delta}(t) + \beta|\dot{\delta}(t)|\dot{\delta}(t) + K_w\,\delta(t) - J_g\,\dot{\varphi}(t)\,\dot{\varepsilon}(t)\,\cos\big(\varepsilon(t)\big) + \int_0^t \dot{\delta}(\tau)\,h(t-\tau)\,d\tau$$

This is an integro-differential equation and it is known as Cummins' equation [12]. The variable $\tau_w(t)$ denotes the wave induced torque on the floater, I_h is the ISWEC moment of inertia around the pitch δ-axis, μ_∞ is the instantaneous added mass, K_w is the linear hydrostatic stiffness and β is the Morison viscous quadratic coefficient. Coefficients β and K_w are computed by means of the hydrodynamic tool AQWA Ansys©.

It is possible to apply a simplification to the introduced dynamic equations [15]. In particular it is possible to describe the ISWEC dynamics with a valid approximation by considering two degrees of freedom only, one related to the pitch dynamics of the hull, and the other related to the precession motion of the gyroscope. Therefore the ISWEC behaviour can be described by the following equations (2.1) and (2.2).

$$T_\varepsilon(t) = I_g\,\ddot{\varepsilon}(t) + J_g\,\dot{\varphi}(t)\,\dot{\delta}(t)\cos\big(\varepsilon(t)\big) \tag{2.1}$$

$$\tau_w(t) = (I_h + \mu_\infty)\ddot{\delta}(t) + \beta|\dot{\delta}(t)|\dot{\delta}(t) + K_w\,\delta(t) - J_g\,\dot{\varphi}(t)\,\dot{\varepsilon}(t)\,\cos\big(\varepsilon(t)\big) + \int_0^t \dot{\delta}(\tau)\,h(t-\tau)\,d\tau \tag{2.2}$$

Focusing on (2.1) it is important to notice that the external torque $T_\varepsilon(t)$ is the torque imposed by the PTO unit controlled by the MPC controller. The last term in the equation represents the induced torque on the gyroscope due to the *gyroscopic effect* phenomenon, already discussed.

The convolution integral in equation (2.3) describes the hydrodynamics radiation force memory effects.

$$\mu(t) = \int_0^t \dot{\delta}(\tau)\,h(t-\tau)\,d\tau \tag{2.3}$$

The angular momentum $J_g\dot{\varphi}(t)$, which causes the induced precession motion, represents the coupling term between the two equations (2.1) and (2.2), thus the coupling between hull pitching motion and the induced gyroscope precession.

2.3 Linearized Model

For control purposes a linear model of the ISWEC system is required. Starting from equations (2.1) and (2.2) it is possible to apply a linearization in the neighborhood of the equilibrium position corresponding to $\varepsilon = 0$ and $\delta = 0$. Moreover, the flywheel is supposed to spin at a constant speed $\dot{\varphi} = \overline{\dot{\varphi}} = const.$

The linearization of the first dynamic equation (2.1) gives:

$$T_\varepsilon(t) = I_g\,\ddot{\varepsilon}(t) + J_g\,\overline{\dot{\varphi}}\,\dot{\delta}(t) \tag{2.4}$$

For the linearization of second dynamic equation (2.2) a particular attention is required for the convolution integral $\mu(t)$, already reported in equation (2.3). According to the procedure discussed in [13] the convolution integral (2.3) can be approximated by an LTI system modelled as the state-space representation

$$\mu(t) = \int_0^t \dot{\delta}(\tau)\, h(t-\tau)\, d\tau \cong \begin{cases} \dot{\rho}_{rv}(t) = \boldsymbol{A}_\rho\, \boldsymbol{\rho}_{rv}(t) + \boldsymbol{B}_\rho\, \dot{\delta}(t) \\ \mu(t) = \boldsymbol{C}_\rho\, \boldsymbol{\rho}_{rv}(t) \end{cases} \tag{2.5}$$

where

$$\boldsymbol{\rho}_{rv}(t) = \begin{bmatrix} \rho_{rv,1}(t), & \dots, & \rho_{rv,\nu}(t) \end{bmatrix}^T \in \mathbb{R}^\nu$$

is the *radiation force dynamic state*, and the matrices $\boldsymbol{A}_\rho$, $\boldsymbol{B}_\rho$ and $\boldsymbol{C}_\rho$ are defined as follows:

$$\boldsymbol{A}_\rho = \begin{bmatrix} a_1 & a_2 & a_3 & \dots & a_\nu \\ 1 & 0 & 0 & \dots & 0 \\ 0 & 1 & 0 & \dots & 0 \\ \vdots & \ddots & \ddots & \ddots & \vdots \\ 0 & \dots & 0 & 1 & 0 \end{bmatrix}, \quad \boldsymbol{B}_\rho = \begin{bmatrix} 1 \\ 0 \\ 0 \\ \vdots \\ 0 \end{bmatrix}$$

$$\boldsymbol{C}_\rho = \begin{bmatrix} c_1 & c_2 & c_3 & \dots & c_\nu \end{bmatrix}$$

A suitable choice for the value of ν which results in valid approximation is $\nu = 4$, [10].

According to the approximation introduced in (2.5) the linearization of the second dynamic equation (2.2) gives:

$$\tau_w = (I_h + \mu_\infty)\ddot{\delta}(t) + K_w\, \delta(t) - J_g\, \overline{\dot{\varphi}}\, \dot{\varepsilon}(t) + \boldsymbol{C}_\rho\, \boldsymbol{\rho}_{rv}(t) \tag{2.6}$$

The state vector $\boldsymbol{x}(t)$ can be thus defined as

$$\boldsymbol{x}(t) = \begin{bmatrix} \dot{\varepsilon}(t) & \varepsilon(t) & \dot{\delta}(t) & \delta(t) & \rho_{rv,1}(t) & \rho_{rv,2}(t) & \rho_{rv,3}(t) & \rho_{rv,4}(t) \end{bmatrix}^T \tag{2.7}$$

Consequently the ISWEC linearized dynamic equations (2.4) and (2.6) can be expressed through the following state-space representation:

$$\dot{\boldsymbol{x}}(t) = \boldsymbol{A}\, \boldsymbol{x}(t) + \boldsymbol{B}\, T_\varepsilon(t) + \boldsymbol{B}_d\, \tau_w(t) \tag{2.8}$$

The matrices $\boldsymbol{A}$, $\boldsymbol{B}$, and $\boldsymbol{B}_d$ are defined as follows.

$$\boldsymbol{A} = \begin{bmatrix} 0 & 0 & -\dfrac{J_g\,\overline{\dot{\varphi}}}{I_g} & 0 & 0 & 0 & 0 & 0 \\ 1 & 0 & 0 & 0 & 0 & 0 & 0 & 0 \\ \dfrac{J_g\,\overline{\dot{\varphi}}}{I_{eq}} & 0 & 0 & -\dfrac{k_w}{I_{eq}} & -\dfrac{c_1}{I_{eq}} & -\dfrac{c_2}{I_{eq}} & -\dfrac{c_3}{I_{eq}} & -\dfrac{c_4}{I_{eq}} \\ 0 & 0 & 1 & 0 & 0 & 0 & 0 & 0 \\ 0 & 0 & 1 & 0 & a_{11} & a_{12} & a_{13} & a_{14} \\ 0 & 0 & 0 & 0 & 1 & 0 & 0 & 0 \\ 0 & 0 & 0 & 0 & 0 & 1 & 0 & 0 \\ 0 & 0 & 0 & 0 & 0 & 0 & 1 & 0 \end{bmatrix} \tag{2.9}$$

$$\boldsymbol{B} = \begin{bmatrix} \dfrac{1}{I_g} & 0 & 0 & 0 & 0 & 0 & 0 & 0 \end{bmatrix}^T \tag{2.10}$$

$$\boldsymbol{B}_d = \begin{bmatrix} 0 & 0 & \dfrac{1}{I_{eq}} & 0 & 0 & 0 & 0 & 0 \end{bmatrix}^T \tag{2.11}$$

where $I_{eq} = I_h + \mu_\infty$.

The linearized ISWEC model (2.8) represents the *state-space model* of the ISWEC which can be used for control purposes. The variable $T_\varepsilon(t)$ is the manipulable input, usually identified by the letter $u(t)$. The variable $\tau_w(t)$ is the applied torque by the incoming wave on the hull about the pitch axis δ and it is considered as a *disturbance* as it is a not manipulable input.

2.4 Contraints

The ISWEC system is subject to some constraints which are mainly due to the PTO limitations. In particular the main constraint relates to the maximum and minimum torque that the PTO electric motor is able to exert, respectively referred to as $T_{\varepsilon_{max}}$ and $T_{\varepsilon_{min}}$. These are crucial values as they affects the capability of the PTO of damping the precession motion and therefore they affect the power harvesting results.
These two limit values are imposed by the electric motor specifics which implement the PTO used in the considered ISWEC system.
A second constraint relates to the maximum allowed angular speed of the PTO shaft, in both clockwise and counter-clockwise direction, respectively referred to as $\dot{\varepsilon}_{max}$ and $\dot{\varepsilon}_{min}$. These constraints come from the maximum voltage supported by the electronic devices implemented in the PTO unit.

As far as the constraints $T_{\varepsilon_{max}}$ and $T_{\varepsilon_{min}}$ are concerned these are respectively defined as:

- $T_{\varepsilon_{max}} = +5000\,\mathrm{Nm}$;
- $T_{\varepsilon_{min}} = -5000\,\mathrm{Nm}$.

An important aspect to be considered is the presence of a gearbox mounted between the PTO unit and the gyroscope shaft. Figure 2.2 shows the configuration. The block M represents the electric motor exerting the command torque on the precession axis ε, whereas the block GB is the gearbox, whose function is to increase the torque and reduce the angular speed of a factor 1:10, from the PTO side to the gyroscope system side.

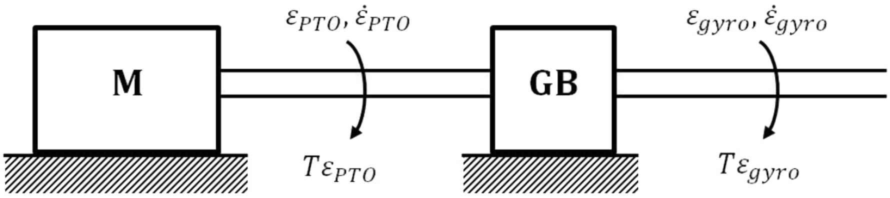

Figure 2.2: PTO Mechanical Configuration

The variables relations resulting from the shown configuration is the following.

- $T_{\varepsilon_{gyro}} = 10 \cdot T_{\varepsilon_{PTO}}$
- $\dot{\varepsilon}_{gyro} = \dot{\varepsilon}_{PTO} \,/\, 10$

The variable $T_{\varepsilon_{gyro}}$ in figure 2.2 is the actual command torque $T_\varepsilon(t)$, whereas the variables ε_{gyro} and $\dot{\varepsilon}_{gyro}$ are respectively the discussed states $\varepsilon(t)$ and $\dot{\varepsilon}(t)$.

The last aspect to be taken into account is that, as already introduced, the considered model implemented in Simulink environment implements only one gyroscope system, whereas the ISWEC system implements two gyroscope systems. As already said it is possible to cast a system composed of two gyroscopes to a single equivalent gyroscope system. As far as the equivalent model is concerned, the $T_{\varepsilon_{max}}$ and $T_{\varepsilon_{min}}$ constraints values to be set up in the MPC control problem are doubled.

Finally, considering the constraints $T_{\varepsilon_{max}}$ and $T_{\varepsilon_{min}}$ toghether with the gearbox and the equivalent model, the MPC controller has to be designed such that can guarantee that the computed command action $T_\varepsilon(t)$ satisfies the relation

$$|T_\varepsilon(t)| \leq \overline{T_\varepsilon}, \quad \forall t \geq 0$$

with $\overline{T_\varepsilon} = 100$ kNm.

As far as the angular speed constraints of the PTO shaft are concerned these are defined as:

- $\dot{\varepsilon}_{max} = +50$ rpm;
- $\dot{\varepsilon}_{min} = -50$ rpm.

These two angular speed limits, related to the state $\dot{\varepsilon}(t)$, are constraints not required to be explicitly taken into account in the MPC control problem as the state $\dot{\varepsilon}(t)$ is minimized by the MPC controller optimization. As consequence of this, later shown in the results sections of control chapter 3, the PTO shaft angular speed behaviour results to assume in nominal conditions values which are much below its constraints. Moreover, in very few and singular cases when the state $\dot{\varepsilon}(t)$ reaches its greatest values, these result to be just close to the mentioned limits, and this does not represent a risk for the proper behaviour of the system. For these reasons the state $\dot{\varepsilon}(t)$ is assumed to behave properly and taking its constraints explicitly into account is not required.

2.5 Control Requirements and Power Extraction

The main requirement which the MPC controller is supposed to accomplish is the maximization of the produced electric power. This task can be realized by considering the mechanical power $P_{PTO}(t)$ defined as

$$P_{PTO}(t) = \dot{\varepsilon}(t) \cdot T_{\varepsilon}(t) \tag{2.12}$$

It is important to notice that the quantity $P_{PTO}(t)$ is a power absorbed by the system provided by the external environment. Therefore a power produced by the system extracted from the external environment is characterized to be a negative quantity. This implies that the quantity $P_{PTO}(t)$ has to be minimized by the MPC controller in order to be as negative as possible during time.

A negative quantity of the power $P_{PTO}(t)$ is obtained by damping the gyroscope shaft precession motion through a given command action $T_{\varepsilon}(t)$ provided by a suitable feedback control law.
Moreover, the computed command action $T_{\varepsilon}(t)$ is supposed to let the gyroscope system assume an oscillating behaviour around $\varepsilon = 0$, thus avoiding complete revolutions, despite mechanically feasible.
In addition the values of the PTO shaft angular speed $\dot{\varepsilon}(t)$ should be minimized to reduce wear and solicitations on the PTO gearbox and power driveline.
Furthermore, for optimizing the energy production, the control energy effort spent by the PTO torque action must be minimized.

The discussed requirements are summarized in the following list:

- R_1: minimization of the absorbed power $P_{PTO}(t)$;
- R_2: zero regulation of the precession motion oscillation described by $\varepsilon(t)$;
- R_3: minimization of the PTO angular speed $\dot{\varepsilon}(t)$ values;
- R_4: minimization of the control energy effort $T_{\varepsilon}^2(t)$.

In order to have a suitable power harvesting performance the command action $T_{\varepsilon}(t)$ shall realize the optimal tradeoff among the four requirements $R_1 \div R_4$, and the model predictive control technique results to be a suitable control strategy for accomplishing such a task.

Chapter 3

MPC Control for ISWEC

In this chapter it is addressed the MPC control technique applied for controlling the ISWEC system with the main task of maximizing the produced electric power. The chapter opens introducing the basics of MPC theory presenting the fundamental notions. Afterwards, the MPC control technique is applied for designing an MPC controller suited to fulfil the ISWEC system requirements. In particular three different versions of MPC are designed. The first MPC controller designed is the main one as the others implement some improvements relying on this version. The second developed MPC controller provides an upgrade by using an augmented model as prediction model which allows to account for the wave contribution into the dynamics. The last developed MPC is characterized for using a more sophisticated prediction model which allows to better foresee the future dynamics of the system.

3.1 Introduction to MPC

MPC stands for *Model Predictive Control* and it is a control technique based on *optimal control* approach. In particular the MPC technique exploits a given dynamic *model* of the plant to be controlled to perform a *prediction* of its states evolution and accordingly computing the *optimal* control action.
MPC technique makes use of optimization algorithms that besides the computation of the optimal command action allow also to take into account given *constraints* of the system, that can be specified in the control problem through mathematical relations. Thus, the control action provided by the MPC controller is such that drives the system to accomplish the specified requirements, fulfilling at the same time the specified constraints.

3.1.1 MPC control problem

The MPC control technique takes place in the discrete-time domain and in particular, a controller based on this technique, computes the optimal command action at each sampling time T_s by performing cyclically the following steps:

- Solving the QP *(Quadratic Programme)* problem;
- Applying the RH *Receding Horizon* principle.

The concepts of *Quadratic Programme* and *Receding Horizon* are hereafter presented.

3.1.2 Quadratic Programme

Solving a *Quadratic Programme* problem means finding the *minimum* (or *maximum*) of a *quadratic function* in the presence of *linear inequality constraints*.

A QP problem can be defined as follows:

$$
\begin{aligned}
&\min_{U(k|k)} J\big(\boldsymbol{x}(k|k), U(k|k)\big) \\
&\textit{Subject To}: \\
&\boldsymbol{x}(k+1) = \boldsymbol{A}\,\boldsymbol{x}(k) + \boldsymbol{B}\,u(k) \\
&u_{min} \leq u(k+i|k) \leq u_{max}\,,\; i = 0, \dots, H_p - 1
\end{aligned}
\tag{3.1}
$$

Where the function $J(\cdot)$ is known as *cost function* and it is defined as:

$$
\begin{aligned}
J\big(\boldsymbol{x}(k|k), U(k|k)\big) = &\,\boldsymbol{x}^T(k+H_p|k)\,\boldsymbol{P}\,\boldsymbol{x}(k+H_p|k) + \sum_{i=0}^{H_p-1} \boldsymbol{x}^T(k+i|k)\,\boldsymbol{Q}\,\boldsymbol{x}(k+i|k) \\
&+ u^T(k+i|k)\,\boldsymbol{R}\,u(k+i|k)
\end{aligned}
\tag{3.2}
$$

and:

- $\boldsymbol{x}(k|k)$ is the measured state in the current instant k;
- $\boldsymbol{x}(k+i|k)$ is the i^{th} step ahead state prediction, basing on the knowledge of the state in the current instant k;
- The variable $U(k|k)$ is the sequence of the applied command actions to be optimized, defined as $U(k|k) = \big[u(k|k),\quad u(k+1|k),\quad u(k+2|k),\quad \dots,\quad u(k+H_p-1|k)\big]^T$;
- H_p is the *prediction horizon* and it is a design parameter which tunes how long in the future the MPC controller will predict the states evolution;
- $\boldsymbol{x}(k+1) = \boldsymbol{A}\,\boldsymbol{x}(k) + \boldsymbol{B}\,u(k)$ is the *prediction model* used by the *MPC* for predicting the states evolution of the system, where $\boldsymbol{x}(k) \in \mathbb{R}^{n\times n}$ and $u(k) \in \mathbb{R}^{n_u\times n_u}$, with n defining the *system order* and n_u defining the *input order*;
- The matrices $\boldsymbol{Q}$, $\boldsymbol{R}$ and $\boldsymbol{P}$ are referred to as *weight matrices*, and are design parameters tuned to find a suitable tradeoff between states tracking and command effort, achieving a behaviour of the system that is as close as possible to the desired one;
- The variables u_{max} and u_{min} are the constraints of the system, where $u_{max} \in \mathbb{R}^{n_u\times n_u}$ and $u_{min} \in \mathbb{R}^{n_u\times n_u}$. These constraints are related respectively to the maximum and minimum command action that the actuator is be able to exert. Nevertheless constraints can be referred to other variables such as the states or the output of the system.

As far as the *cost function* is concerned it is possible to observe that this depends on all the sequence of command actions $U(k|k)$, and on the state in the current instant k only. This is due to the fact that all the future predicted states, which are those from $\boldsymbol{x}(k+1|k)$ to $\boldsymbol{x}(k+H_p|k)$, can be all expressed in terms of the measured current state $\boldsymbol{x}(k|k)$ only and the complete sequence of command actions $U(k|k)$. In particular the i^{th}-step ahead state prediction is given by

$$\boldsymbol{x}(k+i|k) = \boldsymbol{A}^i\,\boldsymbol{x}(k|k) + \boldsymbol{A}^{i-1}\,\boldsymbol{B}\,u(k|k) + \boldsymbol{A}^{i-2}\,\boldsymbol{B}\,u(k+1|k) + \cdots + \boldsymbol{B}\,u(k+i-1|k)$$

The solution of the problem (3.1) gives the optimal sequence of command actions $U^*(k|k)$, shown in equation (3.3), which implements the sequence of command actions that according to the measured current state $\boldsymbol{x}(k|k)$ will drive the system to the desired behaviour according to the tuned design parameters.

$$U^*(k|k) = \big[u^*(k|k), \quad u^*(k+1|k), \quad u^*(k+2|k), \quad \ldots, \quad u^*(k+H_p-1|k)\big]^T \tag{3.3}$$

The sequence $U^*(k|k)$ is referred to as *minimizer* and it is given by

$$arg \min_{U(k|k)} J\big(\boldsymbol{x}(k|k), U(k|k)\big)$$

and is computed by optimizing the predicted state response

$$\boldsymbol{x}(k+1|k),\, \boldsymbol{x}(k+2|k),\, \ldots,\, \boldsymbol{x}(k+H_p|k)$$

obtained on the basis of the current measured state $\boldsymbol{x}(k|k)$.

Simplifying the notation as

$$\boldsymbol{x}(k|k) \equiv \boldsymbol{x}(k), \quad U(k|k) \equiv U(k)$$

and denoting with $X(k)$ the predicted states vector

$$X(k) = \begin{bmatrix} \boldsymbol{x}(k+1) \\ \boldsymbol{x}(k+2) \\ \vdots \\ \boldsymbol{x}(k+H_p) \end{bmatrix}$$

it is possible to write the compact form

$$X(k) = \mathcal{A}\,\boldsymbol{x}(k) + \mathcal{B}\,U(k) \tag{3.4}$$

where:

$$\mathcal{A} = \begin{bmatrix} \boldsymbol{A} \\ \boldsymbol{A}^2 \\ \vdots \\ \boldsymbol{A}^{H_p} \end{bmatrix} \in \mathbb{R}^{n \cdot H_p \times n}, \quad \mathcal{B} = \begin{bmatrix} \boldsymbol{B} & 0 & \ldots & 0 \\ \boldsymbol{AB} & \boldsymbol{B} & \ldots & 0 \\ \vdots & \vdots & \ddots & \vdots \\ \boldsymbol{A}^{H_p-1}\boldsymbol{B} & \boldsymbol{A}^{H_p-2}\boldsymbol{B} & \ldots & \boldsymbol{B} \end{bmatrix} \in \mathbb{R}^{n \cdot H_p \times H_p}$$

Defining:

$$\mathcal{Q} = \begin{bmatrix} \boldsymbol{Q} & 0 & \dots & 0 \\ 0 & \ddots & \ddots & \vdots \\ \vdots & \ddots & \boldsymbol{Q} & 0 \\ 0 & \dots & 0 & \boldsymbol{P} \end{bmatrix} \in \mathbb{R}^{n \cdot H_p \times n \cdot H_p}, \quad \mathcal{R} = \begin{bmatrix} \boldsymbol{R} & 0 & \dots & 0 \\ 0 & \ddots & \ddots & \vdots \\ \vdots & \ddots & \boldsymbol{R} & 0 \\ 0 & \dots & 0 & \boldsymbol{R} \end{bmatrix} \in \mathbb{R}^{n_u \cdot H_p \times n_u \cdot H_p}$$

The *cost function* defined in (3.2) can be expressed in the compact form

$$J\big(\boldsymbol{x}(k), U(k)\big) = X^T(k)\, \mathcal{Q}\, X(k) + U^T(k)\, \mathcal{R}\, U(k) \tag{3.5}$$

Substituting (3.4) in (3.5) the *cost function* can be written in the standard quadratic form, defined as

$$J\big(\boldsymbol{x}(k), U(k)\big) = \frac{1}{2}\, U^T(k)\, \mathcal{H}\, U(k) + \boldsymbol{x}^T(k)\, \mathcal{F}\, U(k) + \overline{\mathcal{J}}$$

where:

- $\mathcal{H} = 2\, \mathcal{B}^T \mathcal{Q}\, \mathcal{B} + \mathcal{R} \succ 0$ is the Hessian matrix of the quadratic form;
- $\mathcal{F} = 2\, \mathcal{A}^T \mathcal{Q}\, \mathcal{B}$ is the mixed term matrix of the quadratic form;
- $\overline{\mathcal{J}} = \boldsymbol{x}^T(k)\, \mathcal{A}^T \mathcal{Q}\, \mathcal{A}\, \boldsymbol{x}(k)$ is the constant term of the quadratic form.

As far as *constraints* are concerned these can be expressed in the QP problem as a matrix inequality relation. Input constraints are considered, but also constraints related to states or output can be considered as well by following the same methodology hereafter presented.

Considering the *constraints* defined in the QP problem (3.1)

$$u_{min} \leq u(k+i|k) \leq u_{max}\,,\; i = 0, \dots, H_p - 1$$

these can be reformulated in a matrix inequality relation as follows:

$$\underbrace{\begin{bmatrix} u(k|k) \\ u(k+1|k) \\ \vdots \\ u(k+H_p-1|k) \end{bmatrix}}_{U(k|k)} \leq \begin{bmatrix} u_{max} \\ u_{max} \\ \vdots \\ u_{max} \end{bmatrix} \Rightarrow \underbrace{\begin{bmatrix} 1 & 0 & \dots & 0 \\ 0 & 1 & \ddots & \vdots \\ \vdots & \ddots & \ddots & \vdots \\ 0 & \dots & \dots & 1 \end{bmatrix}}_{I_{H_p}} \underbrace{\begin{bmatrix} u(k|k) \\ u(k+1|k) \\ \vdots \\ u(k+H_p-1|k) \end{bmatrix}}_{U(k|k)} \leq \begin{bmatrix} u_{max} \\ u_{max} \\ \vdots \\ u_{max} \end{bmatrix}$$

$$\begin{bmatrix} u_{min} \\ u_{min} \\ \vdots \\ u_{min} \end{bmatrix} \leq \underbrace{\begin{bmatrix} u(k|k) \\ u(k+1|k) \\ \vdots \\ u(k+H_p-1|k) \end{bmatrix}}_{U(k|k)} \Rightarrow - \underbrace{\begin{bmatrix} 1 & 0 & \dots & 0 \\ 0 & 1 & \ddots & \vdots \\ \vdots & \ddots & \ddots & \vdots \\ 0 & \dots & \dots & 1 \end{bmatrix}}_{I_{H_p}} \underbrace{\begin{bmatrix} u(k|k) \\ u(k+1|k) \\ \vdots \\ u(k+H_p-1|k) \end{bmatrix}}_{U(k|k)} \leq \begin{bmatrix} -u_{min} \\ -u_{min} \\ \vdots \\ -u_{min} \end{bmatrix}$$

Rearranging the given linear constraints on $U(k|k)$ it is possible to write

$$\underbrace{\begin{bmatrix} I_{H_p} \\ \\ -I_{H_p} \end{bmatrix}}_{G_u} \underbrace{\begin{bmatrix} u(k|k) \\ \vdots \\ u(k+H_p-1|k) \end{bmatrix}}_{U(k|k)} \leq \underbrace{\begin{bmatrix} u_{max} \\ \vdots \\ u_{max} \\ -u_{min} \\ \vdots \\ -u_{min} \end{bmatrix}}_{h_u} \Rightarrow G_u\, U(k|k) \leq h_u$$

Finally, the QP problem can be expressed in the standard quadratic form as

$$\begin{aligned} & U^*(k|k) = arg \min_{U(k|k)} \frac{1}{2}\, U^T(k)\, \mathcal{H}\, U(k) + \boldsymbol{x}^T(k)\, \mathcal{F}\, U(k) + \overline{\mathcal{J}} \\ & \textit{Subject To}: \\ & G_u\, U(k|k) \leq h_u \end{aligned} \tag{3.6}$$

Many efficient algorithms exist to solve a convex QP problem expressed as the one in (3.6), as:

- *Active-Set* algorithms;
- *Interior-Point* algorithms.

3.1.3 Receding Horizon

As seen solving the problem (3.1) means finding a sequence of command actions $U(k)$ that minimize the cost function $J(\boldsymbol{x}(k), U(k))$. The control actions applied in this way, though, would arise an *open-loop* control strategy, because the command actions $U(k)$ are based on the measure of the state $\boldsymbol{x}(k)$ in the current instant k only, and thus do not take into account further measures of the state in the next sampling times. This problem could lead to misbehaviours given by uncertainties and disturbances on the system.
The problem is addressed by introducing the *receding horizon* technique, which consists in iterating at each sampling time T_s the following procedure.

Receding horizon technique:

I) Measurement of the state $\boldsymbol{x}(k)$ in the current instant k;

II) Solving the QP problem (3.1);

III) Computation of the minimizer $U^*(k) = \begin{bmatrix} u^*(k), & u^*(k+1), & u^*(k+2), & \ldots, & u^*(k+H_p-1) \end{bmatrix}^T$;

IV) Application of the first command action only, i.e. $u^*(k)$;

V) Repeating the procedure at the next sampling time $k \rightarrow k+1$.

Using this technique the MPC controller accomplishes a *closed-loop* control strategy, as the state $\boldsymbol{x}(k)$ is measured at each sampling time. Therefore, by adopting the receding horizon principle the controller is capable of sensing the state evolution at each sampling time T_s and accordingly to react to possible uncertainty errors and unpredicted disturbances.

Moreover, the case where the system model and cost function are time-invariant leads to an implicit definition of an *nonlinear time-invariant static state-feedback control law* of the form

$$u(k) = \mathcal{K}\big(\boldsymbol{x}(k)\big)$$

The figure 3.1 illustrates the Receding Horizon control strategy.

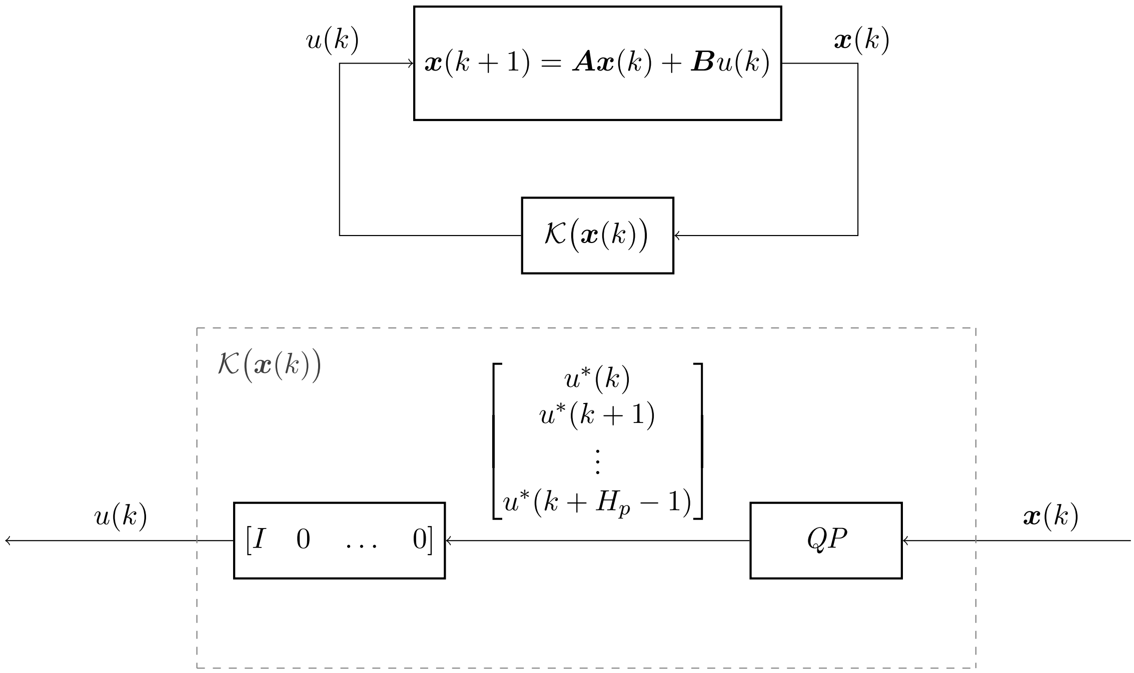

Figure 3.1: Receding Horizon - Block Diagram

3.1.4 Feasibility and Stability of MPC

Feasibility guarantees that the QP problem can be solved at each sampling time T_s.
A QP problem defined as the one in (3.6) can be always solved provided that it is a convex one. Constraints defined only on the input $u(k)$ imply convexity of the problem and thus guarantee always a solution, whereas if the QP problem also includes constraints on the output or some state it is not guaranteed to provide a solution.

Infeasibility could also arise due to:

- Modelling errors;
- Presence of disturbance;
- Wrong design setup, (e.g. $\boldsymbol{Q}$, $\boldsymbol{R}$, H_p).

As far as stability of the system is concerned, this depends on the defined $\boldsymbol{Q}$, $\boldsymbol{R}$, H_p and constraints. A wrong tuning of these parameters may thus lead the system to instability. The prediction horizon parameter H_p can be used for stabilizing the system behaviour. In particular, in case of instability, higher values of H_p can stabilize the system behaviour, with the drawback of increasing the complexity of the problem and the required computational effort.

3.1.5 Tuning of Weight Matrices

The desired behaviour of the system to be controlled can be achieved, as close al possible, by tuning the the weight matrices $\boldsymbol{Q}$, $\boldsymbol{P}$ and $\boldsymbol{R}$ of the problem (3.1), besides other parameters later discussed.
As it is possible to notice in the *cost function* (3.2) the matrix $\boldsymbol{Q}$ is related to states optimization whereas the matrix $\boldsymbol{R}$ is related to the command action optimization.

Matrices $\boldsymbol{Q}$, $\boldsymbol{P}$ and $\boldsymbol{R}$ are diagonal matrices, and their entries define the *penalty* on the optimization variable their are related to. In particular:

- $\boldsymbol{Q} = \boldsymbol{Q}^T \succeq 0, \quad \boldsymbol{Q} \in \mathbb{R}^{n \times n}$;
- $\boldsymbol{P} = \boldsymbol{P}^T \succ 0, \quad \boldsymbol{P} \in \mathbb{R}^{n \times n}$;
- $\boldsymbol{R} = \boldsymbol{R}^T \succ 0, \quad \boldsymbol{R} \in \mathbb{R}^{n_u \times n_u}$.

with n and n_u that are respectively the *system order* and the *input order*. Where:

$$\boldsymbol{Q} = \begin{bmatrix} q_{11} & 0 & 0 & \dots & 0 \\ 0 & q_{22} & 0 & \dots & 0 \\ 0 & 0 & q_{33} & \ddots & \vdots \\ \vdots & \vdots & \ddots & \ddots & 0 \\ 0 & 0 & \dots & 0 & q_{nn} \end{bmatrix}, \boldsymbol{R} = \begin{bmatrix} r_{11} & 0 & 0 & \dots & 0 \\ 0 & r_{22} & 0 & \dots & 0 \\ 0 & 0 & r_{33} & \ddots & \vdots \\ \vdots & \vdots & \ddots & \ddots & 0 \\ 0 & 0 & \dots & 0 & r_{n_u n_u} \end{bmatrix}. \tag{3.7}$$

The weights q_{ii} and r_{ii} have the purpose of associating a certain *penalty* to the related *state* or *input* variable to minimize. The higher the weight value the more important is the associated variable for the minimization problem.

As far as $\boldsymbol{Q}$ is concerned each entry of the matrix is associated to a given state, i.e. q_{ii} relates to state $\boldsymbol{x}_i$. An high value on a given state will lead the controller to minimize with high priority the values assumed by that state during its evolution.

Same concept holds for the matrix $\boldsymbol{R}$. Supposing to have $\boldsymbol{R} \in \mathbb{R}$ for sake of simplicity. Low values of $\boldsymbol{R}$ will result in an aggressive command activity, i.e. characterized by high values and fast variations, whereas high values of $\boldsymbol{R}$ will result in a quieter command activity, that means characterized by lower values and slower variations. Choosing low values of $\boldsymbol{R}$ is indicated for obtaining high performances by the systems in terms of transient response, overshoot and settling time. Conversely, high values of $\boldsymbol{R}$ are chosen to reduce energy consumption, with the drawback of obtaining decreased performance.
The matrices $\boldsymbol{Q}$ and $\boldsymbol{R}$ are thus tuned to get a suitable tradeoff between system performance and command effort that best satisfies the desired requirements of the system to control.

As far as the matrix $\boldsymbol{P}$ is concerned this is related to the penalty given to the terminal predicted state $\boldsymbol{x}(k + H_p)$, as shown in the cost function (3.2). This matrix is given by the solution of the Discrete-time Algebraic Riccati Equation (DARE), defined as

$$\boldsymbol{P} = \boldsymbol{A}^T \boldsymbol{P}\, \boldsymbol{A} + \boldsymbol{Q} - \boldsymbol{A}^T \boldsymbol{P}\, \boldsymbol{B}\, (\boldsymbol{R} + \boldsymbol{B}^T \boldsymbol{P}\, \boldsymbol{B})^{-1} \boldsymbol{B}^T \boldsymbol{P}\, \boldsymbol{A}$$

This choice is made to ensure stability of the closed-loop feedback control system.

3.2 MPC for ISWEC

In this section the MPC control technique is addressed for controlling the ISWEC system with the main requirement of maximizing the produced electric power. The system architecture is presented and explained as well as the Simulink model used for simulations. The MPC controller design and the achieved results are shown and discussed.

3.2.1 Control System Architecture

The ISWEC control system architecture is shown in figure 3.2.

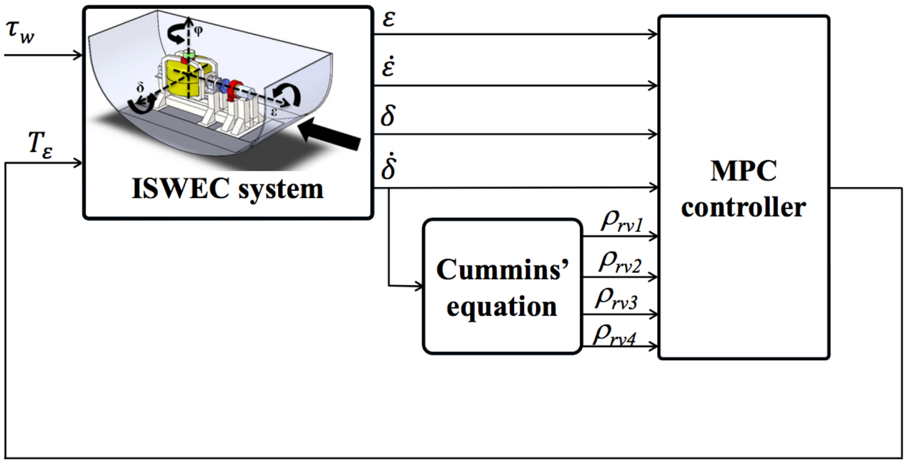

Figure 3.2: Control System Architecture - MPC

It is possible to observe that the ISWEC system takes two inputs, τ_w and T_ε, which are respectively the applied torque by the wave on the hull about the pitch DoF δ, and the PTO command torque computed by the MPC controller. The output of the ISWEC are the four measurable states ε, $\dot{\varepsilon}$, δ and $\dot{\delta}$. The state $\dot{\delta}$ enters in the block referred to as *Cummins' Equation* which is intended to provide the four hydrodynamic states ρ_{rv1}, ρ_{rv2}, ρ_{rv3} and ρ_{rv4} according to the linearized Cummins' equation discussed in chapter 2. The eight available states enter in the MPC controller which accordingly computes the command action T_ε intended for driving the PTO of the ISWEC system.

The Simulink model implementing the discussed architecture is shown in figure 3.3, reported as a full page image for a comfortable visualization. The subsystem *WAVES* in light blue color implements the input of the system. The two green subsystems *HULL* and *GYRO* implement the detailed ISWEC nonlinear model by implementing the ISWEC differential equations introduced in chapter 2. As the names suggest, the *HULL* subsystem is responsible for modelling the nonlinear dynamics of the oscillating hull of the ISWEC system, whereas the *GYRO* subsystem is responsible for modelling the nonlinear dynamics of the gyroscope structure. Thus, these two subsystems are responsible for computing the *states* evolution of the system according to the nonlinear nature of the ISWEC system.
The last subsystem is the *CONTROLLER*, in blue, which implements the MPC control law, taking as input the measurable states and providing in output the command action T_ε, which implements the PTO command torque to be exerted on the gyroscope shaft.

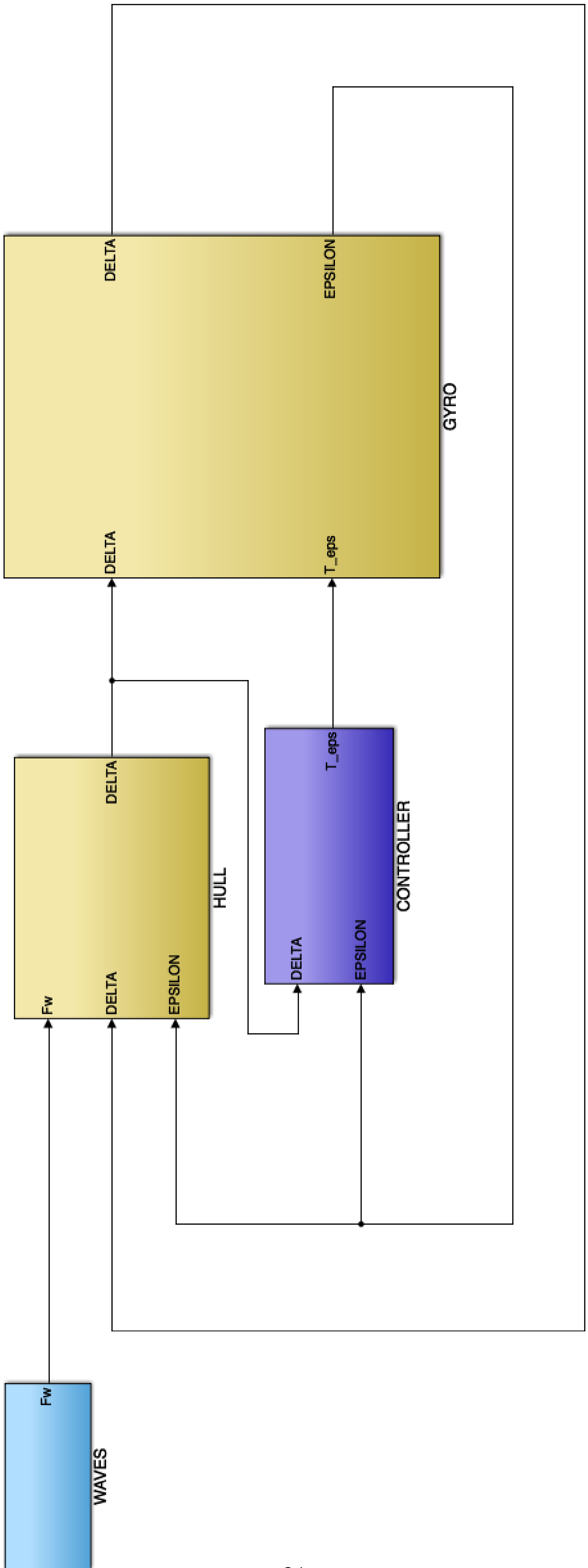

Figure 3.3: Simulink Model - MPC

The signal F_w coming from *WAVES* subsystem implements the wave force source applied to the ISWEC. This signal contains different variables, including τ_w already described in the architecture figure 3.2. Consequently this signal F_w is properly demultiplexed in the subsystems to obtain the required variable τ_w. Both signals *EPSILON* and *DELTA* contain anglular position, angular speed and angular acceleration variables, respectively about the ε-axis of the gyroscope shaft and about δ-axis related to the pitch motion of the hull. These signals are properly demultiplexed and managed inside the Simulink subsystems. It is possible to see that the signals *EPSILON* and *DELTA* are common to both *HULL* and *GYRO* subsystems, as the dynamics of one influences the dynamics of the other and vice-versa through reaction forces. The signal *T_eps* is the optimal command torque T_ε computed by the MPC controller.

The figure 3.4 shows the *CONTROLLER* subsystem which is present in the main block diagram of figure 3.3. It is possible to see that it contains itself two subsystems:

- *Full State Builder*;
- *MPC Controller*.

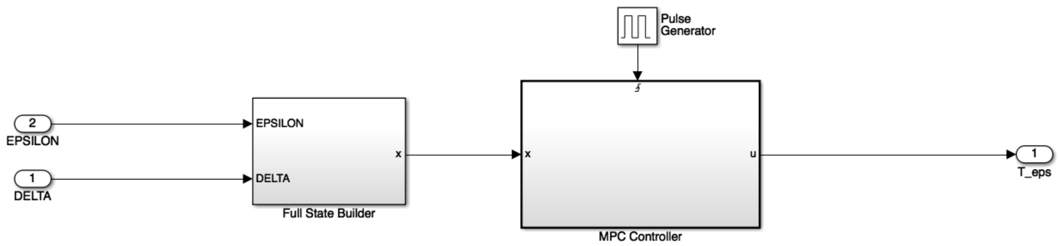

Figure 3.4: Controller Subsystem - MPC

The *Full State Builder* subsystem is intended for accomplishing two tasks.
The first task is providing the 4 hydrodynamic states $\rho_{rv,1}$, $\rho_{rv,2}$, $\rho_{rv,3}$ and $\rho_{rv,4}$ computed from the measure of the state $\dot{\delta}(k)$ by means of the linearized Cummins' equation. The second task is to organize the eight available states such that at any sampling time k the state vector (3.8) is available.

$$\boldsymbol{x}(k) = \begin{bmatrix}\dot{\varepsilon}(k) & \varepsilon(k) & \dot{\delta}(k) & \delta(k) & \rho_{rv,1}(k) & \rho_{rv,2}(k) & \rho_{rv,3}(k) & \rho_{rv,4}(k)\end{bmatrix}^T \tag{3.8}$$

The *MPC Controller* subsystem implements the real MPC controller of the system, which takes the state measure $\boldsymbol{x}(k)$ in input and provides the optimal command action $T_\varepsilon(k)$ in output.

The ISWEC nonlinear model is simulated as a continuous-time system, whereas the *MPC Controller* works in discrete-time domain with sampling time T_s. For this reason a *Pulse Generator* has been introduced in the model for providing a pulse signal with sampling time T_s with the purpose of synchronizing the discrete-time MPC with the running continuous-time ISWEC model. Between two consecutive sampling time instants the command action $T_\varepsilon(k)$ computed by the MPC controller is kept constant.

3.2.2 MPC Control problem

The MPC controller addressed in this context uses as *prediction model* a model that doesn't take into account explicitly the incoming wave and therefore the related induced torque. The incoming wave just excites the pitch dynamics of the hull and accordingly the gyroscope system dynamics by means of the *gyroscope effect* coupling, discussed in the chapter 2. Thus, the controller works measuring the states and computing their prediction without taking into account the contribution of the incoming wave during the prediction. Basing on this prediction the *MPC controller* computes the *optimal* command action $T_\varepsilon(k)$.

The discrete-time *prediction model* used by the MPC controller is the following:

$$\boldsymbol{x}(k+1) = \boldsymbol{A}_{DT}\,\boldsymbol{x}(k) + \boldsymbol{B}_{DT}\,u(k) \tag{3.9}$$

where the *state matrix* $\boldsymbol{A}_{DT}$ and the *input matrix* $\boldsymbol{B}_{DT}$ come from the discretization operation of the continuous-time model in (3.10) using the zero order holder (ZOH) method.

$$\dot{\boldsymbol{x}}(t) = \boldsymbol{A}\,\boldsymbol{x}(t) + \boldsymbol{B}\,u(t) \tag{3.10}$$

The *state matrix* $\boldsymbol{A}$ and the *input matrix* $\boldsymbol{B}$ come from the linearized ISWEC model seen in chapter 2, hereafter reported

$$\mathbf{A} = \begin{bmatrix} 0 & 0 & -\dfrac{J_g\,\overline{\dot{\varphi}}}{I_g} & 0 & 0 & 0 & 0 & 0 \\ 1 & 0 & 0 & 0 & 0 & 0 & 0 & 0 \\ \dfrac{J_g\,\overline{\dot{\varphi}}}{I_{eq}} & 0 & 0 & -\dfrac{k_w}{I_{eq}} & -\dfrac{c_1}{I_{eq}} & -\dfrac{c_2}{I_{eq}} & -\dfrac{c_3}{I_{eq}} & -\dfrac{c_4}{I_{eq}} \\ 0 & 0 & 1 & 0 & 0 & 0 & 0 & 0 \\ 0 & 0 & 1 & 0 & a_{11} & a_{12} & a_{13} & a_{14} \\ 0 & 0 & 0 & 0 & 1 & 0 & 0 & 0 \\ 0 & 0 & 0 & 0 & 0 & 1 & 0 & 0 \\ 0 & 0 & 0 & 0 & 0 & 0 & 1 & 0 \end{bmatrix}, \quad \mathbf{B} = \begin{bmatrix} \dfrac{1}{I_g} \\ 0 \\ 0 \\ 0 \\ 0 \\ 0 \\ 0 \\ 0 \end{bmatrix}$$

According to the control requirements $R_1 \div R_4$ presented in chapter 2 hereafter reported for readability convenience, the *cost function* has been defined in a customized form, reported in (3.11).

Control Requirements of ISWEC system:

- R_1: minimization of the absorbed power $P_{PTO}(t)$;
- R_2: zero regulation of the precession motion oscillation described by $\varepsilon(t)$;
- R_3: minimization of the PTO angular speed $\dot{\varepsilon}(t)$ values;
- R_4: minimization of the control energy effort $T_\varepsilon^2(t)$.

MPC cost function:

$$J(k) = \sum_{k=1}^{H_p-1} q_{11}\,\dot{\varepsilon}^2(k) + q_{22}\,\varepsilon^2(k) + 2\,n_1\,\dot{\varepsilon}(k)\,T_\varepsilon(k) + r\,T_\varepsilon^2(k) \tag{3.11}$$

The peculiarity of the *cost function* (3.11) lies in the presence of a mixed term, which is the one defined as $2\,n_1\,\dot{\varepsilon}(k)\,T_\varepsilon(k)$. This is referred to as mixed term as it involves two different optimization variables in a product fashion, with its given weight. A mixed term is generally not present in a standard cost function, as the one introduced in (3.2).

The presented cost function can be expressed in a general form as:

$$J(k) = \sum_{k=1}^{H_p-1} \begin{bmatrix} \boldsymbol{x}^T(k) & u(k) \end{bmatrix} \begin{bmatrix} \boldsymbol{Q} & \boldsymbol{N} \\ \boldsymbol{N}^T & \boldsymbol{R} \end{bmatrix} \begin{bmatrix} \boldsymbol{x}(k) \\ u(k) \end{bmatrix} \tag{3.12}$$

where in the customized form suited for the ISWEC control the weight matrices are defined as:

$$\boldsymbol{Q} = \begin{bmatrix} q_{11} & 0 & 0 & \dots & 0 \\ 0 & q_{22} & 0 & \dots & 0 \\ 0 & 0 & 0 & \dots & 0 \\ \vdots & \vdots & \vdots & \ddots & \vdots \\ 0 & 0 & 0 & \dots & 0 \end{bmatrix} \in \mathbb{R}^{8\times 8}, \quad \boldsymbol{N} = \begin{bmatrix} n_1 \\ 0 \\ 0 \\ \vdots \\ 0 \end{bmatrix} \in \mathbb{R}^{8\times 1}, \quad \boldsymbol{R} = r \in \mathbb{R} \tag{3.13}$$

Focusing on the cost function defined in (3.11) it's possible to analyse the terms it is composed of:

- The first term whose weight is q_{11} is related to the minimization of the angular speed of the PTO shaft $\dot{\varepsilon}(k)$. This term is thus intended for keeping the PTO shaft angular speed at low values.
- The second term with weight q_{22} is related to the minimization of the angular position of the PTO shaft $\varepsilon(k)$. Therefore this term is the one intended to lead the position of the gyroscope structure to its equilibrium point, i.e. $\varepsilon = 0$, letting the gyroscope system assume an oscillating behaviour around $\varepsilon = 0$.
- The third therm whose weight is n_1 is related to the minimization of the absorbed power. The product $\dot{\varepsilon}(k)\,T_\varepsilon(k)$ is indeed physically a power term, where $\dot{\varepsilon}(k)$ is the angular speed of the PTO shaft and $T_\varepsilon(k)$ is the applied torque to the same PTO shaft.
- The last term with weight r is related to the minimization of the command activity. This term is therefore intended for minimizing the energy spent due to the command actions.

3.2.3 Implementation

The implementation of the MPC controller discussed in the previous subsection has been realized making use of two MATLAB toolboxes, which are:

- MPT3
- YALMIP

The MPT3 toolbox is the main toolbox used for this thesis work. This allows to setup an MPC control problem in a deepened way allowing to customize the various MPC parameters such as weight matrices, prediction model and constraints.
The MPC controller implemented by this toolbox uses the linearized model of the ISWEC system and solves the optimization problem through a Quadratic Programme (QP) algorithm, characterized to be an efficient algorithm from a computational point of view.

As the MPT3 toolbox does not give the possibility to treat a mixed term in the *cost function* $J(\cdot)$ the usage of YALMIP is required. YALMIP toolbox gives the chance to write a customized cost function by writing manually term by term, with the possibility of using any optimization variable involved in the problem. This gives therefore the chance to insert a product of variables, that in this context is required for adding the mixed term related to the minimization of the absorbed power.

More in the details, the usage of the two toolboxes allows to create in MATLAB environment an *MPC object* which implements the MPC controller, characterized by:

- Prediction Model;
- Prediction Horizon H_p;
- Sampling Time T_s;
- Weight Matrices $\boldsymbol{Q}$, $\boldsymbol{N}$, $\boldsymbol{R}$;
- Constraints $T_{\varepsilon_{max}}$ and $T_{\varepsilon_{min}}$.

These are parameters to be tuned and set up. The defined *MPC object* allows to call a function which takes as input a vector containing the measure of the eight states in the instant k providing accordingly the optimal command action $T_\varepsilon(k)$ as a scalar value. This function call is implemented by the MPC controller presented in figure 3.4.

Once the MPC controller object has been created, the furter design step takes place by tuning properly its parameters aiming to find the optimal tradeoff among the system requirement $R_1 \div R_4$.
Numerical simulations of the simulink model in figure 3.3 provide produced power, command activity and state behaviour results which is possible to investigate through graphs and variables storage, allowing thus to understand the proper tuning to set for achieving the desired results.
The first tuning set of the MPC parameters have been chosen according to the theory introduced in this chapter. Consequently the MPC parameters have been tuned and refined through experimental simulations by evaluating the obtained results in post-simulation. The experimental activity, consisting in designing a suitable tuning set for the MPC parameters, has been performed basing on the knowledge of MPC theory and on the experience gathered during the thesis activity.
Moreover, the final tuning design is such that the MPC controller gives optimal results for all the sea state conditions in which the ISWEC system is supposed to work. This last task has been performed by simulating the ISWEC model providing different wave profile as excitation input, as later discussed.
The resulting optimal tuning of the MPC controller parameters suited for the ISWEC system are presented in table 3.1.

Table 3.1: MPC Parameters

Parameter	**Value**	**Description**
T_s	$50\ (ms)$	Sampling Time
H_p	2	Prediction Horizon
q_{11}	$1 \cdot 10^9$	Q matrix weight
q_{22}	$3 \cdot 10^{10}$	Q matrix weight
n_1	1	N matrix weight
r	0.020	R matrix weight
$T_{\varepsilon_{max}}$	$+100\,(\text{kNm})$	Constraint
$T_{\varepsilon_{min}}$	$-100\,(\text{kNm})$	Constraint

The controller sampling time has been set to $T_s = 50\,\text{ms}$ with a prediction horizon $H_p = 2$, which means that the MPC controller performs at each sampling time T_s a prediction of $100\,\text{ms}$ of the system dynamics evolution, by means of the prediction model (3.9).
As seen in chapter 2 the spinning flywheel speed $\dot{\varphi}(t)$ of the gyroscope system has to be set to a constant value $\overline{\dot{\varphi}}$. For all the simulations performed in this thesis work the spinning flywheel speed has been set to $\overline{\dot{\varphi}} = 40\,\text{rad}\,\text{s}^{-1} \cong 382\,\text{rpm}$.

Wave Set

As the ISWEC system is supposed to work in Pantelleria sea, all the possible states in which this sea could be have been characterized and classified in nine different wave profiles, which are reported in table 3.2, where T_e is the energy period, H_s is the significant height, P_s is the power density and f_O represents the wave occurrence rate expressed in percentage value, such that the sum of the occurrence rates of the nine waves results as 100%. As far as the rates f_O are concerned, these have been computed by analysing the presence of a given sea state as hours at year, during the year 2010.

Table 3.2: Wave Set

Wave ID	$T_e\,(s)$	$H_s\,(m)$	$P_s\,(kWm^{-1})$	f_O (%)
1	5.31	1.18	3.65	11.5326
2	6.44	1.97	12.25	12.2144
3	7.38	0.67	1.61	6.4692
4	6.54	0.68	1.50	16.2143
5	6.83	1.36	6.23	10.8416
6	8.09	2.20	19.18	2.1993
7	7.77	1.45	8.06	5.3023
8	7.27	1.99	14.16	7.4865
9	5.36	0.69	1.25	27.7398

Each sea state mentioned in table 3.2 has been sampled and stored in nine respective files called $forcing\_wave$, which implement the actual input of the ISWEC model during simulations.
Each of the mentioned forcing wave vector file contain actually different values. The ones of main interest are the applied torque evolution about the pitch axis of the hull by the wave $\tau_w(k)$, and the time instants k at which a given value of torque is applied. The exact duration of these input wave is 1023.5 s, which means 17.05 min.

An example of wave profile is presented in figure 3.5, which illustrates the time evolution of $\tau_w(k)$ for the wave classified as *Wave 1* in table 3.2.

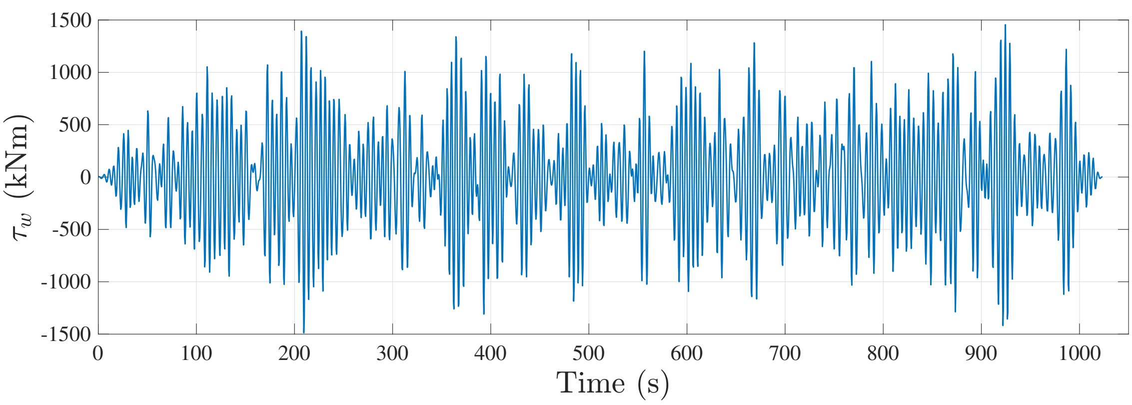

Figure 3.5: Wave Induced Torque (Wave 1)

3.2.4 Results

In this section the results obtained through simulations are presented in order to show the effectiveness of the MPC approach applied to the ISWEC system. Such simulations have been performed using the detailed nonlinear ISWEC model presented in this chapter. The main results in this thesis work are related to the *produced power* by the ISWEC PTO unit with the designed MPC controller, but also *command activity* and system *states behaviour* results are presented.

Produced Power Analysis

The produced power evaluation is made in MATLAB/Simulink environment through numerical simulations of the ISWEC nonlinear model controlled by the designed MPC controller. It is important to remark that in order to obtain a stochastically valid result the ISWEC model has to be simulated for a time interval which lasts about 20 minutes, thus the available input wave stimuli mentioned in the previous subsection can be considered compliant with such a requirement.

Besides other variables afterwards discussed the simulations provide the time evolution of the absorbed power, which is expressed in a structure variable containing both the sequence of values which the absorbed power assumes during the simulation and the time instants in which a given value of the power relates. Therefore it is possible to plot the evolution of the absorbed power by the PTO unit.

The figure 3.6 shows the time evolution of the *absorbed power* by PTO unit of the system when this is excited by the wave profile classified as *Wave 1* in the table 3.2 and shown in figure 3.5.

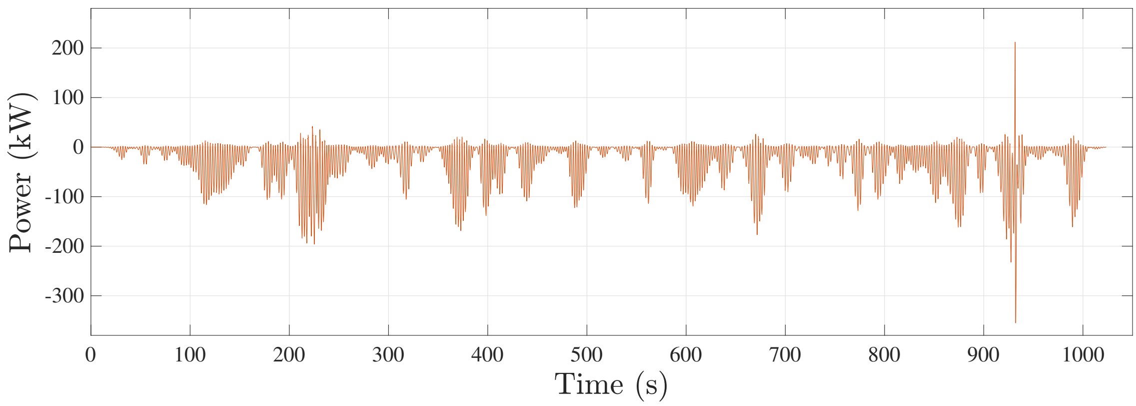

Figure 3.6: Absorbed Power Plot - MPC

It is important to notice that the plot shows the *absorbed power*, and it is possible to see that the power trend is characterized by negative peaks which is the reason why the power is actually produced. As already introduced, when the power given to a system is a negative quantity this power is actually given from the system to the source, which means that it is a produced power.

In order to evaluate the effectiveness of the developed MPC controller the produced power trend has been compared with the one obtained through the simulation of the same ISWEC model when it is controlled by the PD control law introduced in [8] and defined as:

$$T_{\varepsilon}^{PD} = -k \cdot \varepsilon - c \cdot \dot{\varepsilon} \tag{3.14}$$

with

$$k = 100\,\mathrm{kNm\,rad^{-1}}\,, \quad c = 100\,\mathrm{kNms\,rad^{-1}}.$$

It is worth to remark that the control law defined in (3.14) does not handle the constraints and it is therefore needed that the computed command action T_{ε}^{PD} is bounded by means of a saturation for accomplishing the constraints discussed in chapter 2.

Figure 3.7 compares the *absorbed power* trend obtained with the MPC approach with the one obtained with PD approach. The red line identifies the *absorbed power* trend when the PTO is controlled by the MPC controller, whereas the blue line identifies the *absorbed power* trend when it is controlled by the PD.

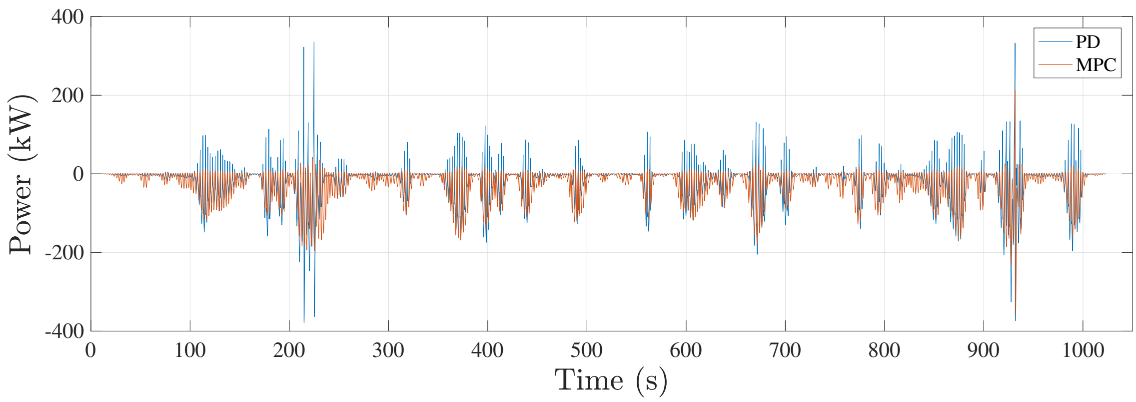

Figure 3.7: Absorbed Power Plot - PD vs MPC

It is possible to observe that the trend of the produced power with the MPC approach results negative for almost its all duration, differently from the case of the PD controller, where it is possible to see several intervals characterized by positive peaks. As already discussed, the positive peaks present in the PD approach represent a lost power since it is actually absorbed by the system. Therefore the presented comparison shows the effectiveness of the MPC approach.

In figure 3.8 it is reported a section of figure 3.7 in which it is possible to make a further observation.This figure can be characterized by two sections according to the sea state. In particular the first section which goes from 0 s to 100 s is characterized by a quieter sea state, whereas the second section which goes from 100 s to 160 s is characterized by a rougher sea state (see figure 3.5). Focusing on the first section where the sea is quieter it is possible to appreciate the capability of the MPC controller to extract much more power than the PD controller is able to do. This can be seen observing the power trend of the MPC in red as it reaches much more negative peaks than the case with PD approach.
The second section of the figure, instead, shows how the produced power trend related to the MPC method reaches smaller spike values with respect to the PD controller one, and this guarantees a more stable power flow in the power electronics of the PTO unit.

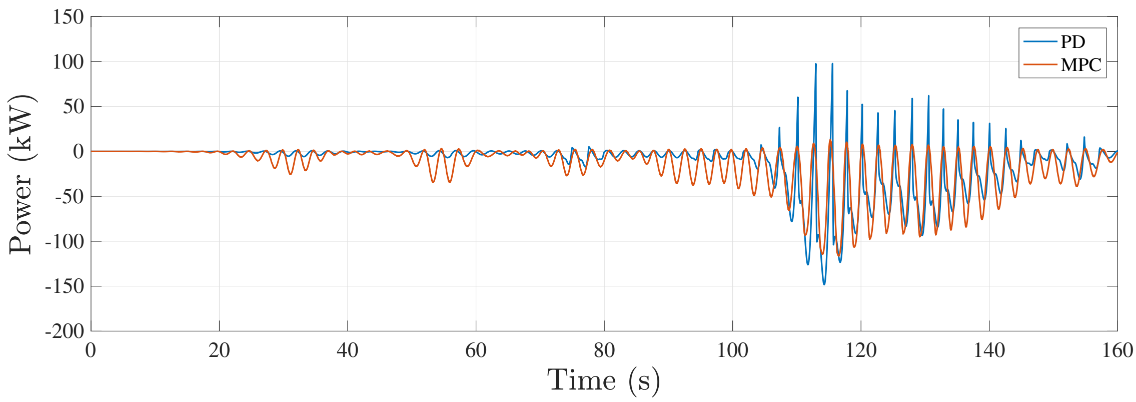

Figure 3.8: Absorbed Power Plot (section) - PD vs MPC

For the power production evaluation it has been considered the *produced mean power* $\overline{P}$ defined as

$$\overline{P} = -\frac{1}{n_s} \sum_{k=1}^{n_s} P(k) \tag{3.15}$$

where n_s is the number of samples of the produced power obtained from the simulation and $P(k)$ is the absorbed power value in the instant k. The *minus* sign is used to get a positive number as the provided result would be negative quantity, as already discussed. The *produced mean power* $\overline{P}$ has been computed for all the nine sea states reported in table 3.2 exciting the ISWEC system controlled by the MPC tuned according to the parameters setting summarized in table 3.1.

Then, the maximum of $\overline{P}_{max}$ over all the obtained values of $\overline{P}$ is evaluated. The productivity comparison between MPC and the PD is performed in terms of the normalized produced mean power $\widehat{P}$ defined as

$$\widehat{P} = \frac{\overline{P}}{\overline{P}_{max}}$$

whose results are reported in table 3.3.

Each row of the table 3.3 reports the wave identification *Wave ID* and the corresponding normalized mean power produced by the PD and MPC control strategies respectively referred to as $\widehat{P}_{PD}$ and $\widehat{P}_{MPC}$.

Table 3.3: Normalized Produced Mean Power - MPC

Wave ID	$\widehat{P}_{PD}$	$\widehat{P}_{MPC}$
1	0.3647	0.4149
2	1.00	0.9787
3	0.0126	0.0552
4	0.0232	0.0794
5	0.2385	0.3037
6	0.2844	0.3669
7	0.063	0.1635
8	0.5058	0.5614
9	0.0696	0.1241

It's possible to appreciate that the MPC approach provides a greater produced power than the PD approach for all the wave profiles, with the exception of the Wave 2, where the produced power by the MPC is still close to the power produced by PD controller.

The histogram in figure 3.9 shows from a graphical point of view the the comparison between the normalized produced mean powers $\widehat{P}_{PD}$ and $\widehat{P}_{MPC}$ for the nine sea states of interest.

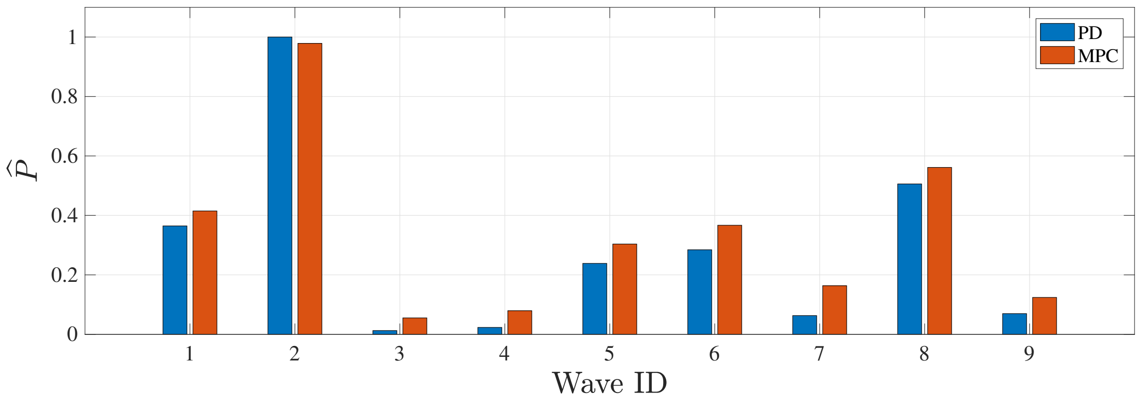

Figure 3.9: Produced Power Histogram

For a quantitative analysis on the produced power increment provided by the MPC approach it is possible to evaluate the percentage increment according to the following formula:

$$\Delta\overline{P} = \frac{\overline{P}_{MPC} - \overline{P}_{PD}}{\overline{P}_{PD}} \cdot 100 \tag{3.16}$$

Results of the formula (3.16) are reported in the following table 3.4.

Table 3.4: Produced Power percentage increment - MPC

Wave ID	$\Delta\overline{P}$ (%)
1	$+13.79$
2	-2.13
3	$+337.27$
4	$+242.33$
5	$+27.32$
6	$+28.99$
7	$+159.68$
8	$+10.97$
9	$+78.34$

According to values of *produced mean power* $\overline{P}$ computed through the formula (3.15) and the nine wave rate occurrences reported in table 3.2 it is possible to compute the *yearly energy production* E_{year} expressed in MW per year, according to the following formula

$$E_{year} = \frac{8760}{1000} \sum_{i=1}^{9} \overline{P_i} \cdot \frac{f_{O_i}}{100} \tag{3.17}$$

Referring to the yearly produced energy by PD and MPC approaches respectively as E_{year}^{PD} and E_{year}^{MPC}, it is possible to compute the normalized yearly produced energies $\widehat{E}_{year}^{PD}$ and $\widehat{E}_{year}^{MPC}$, whose results are reported in table 3.5

Table 3.5: Normalized Yearly Energy Production - MPC

$\widehat{E}_{year}^{PD}$	$\widehat{E}_{year}^{MPC}$
0.843	1.00

It is possible to compute the percentage increment of the yearly energy production provided by the MPC approach according to the formula

$$\Delta E_{year}^{MPC} = \frac{E_{year}^{MPC} - E_{year}^{PD}}{E_{year}^{PD}} \cdot 100$$

which provides

$$\Delta E_{year}^{MPC} = 18.59\,\%$$

Thus, the yearly energy production increment ΔE_{year}^{MPC} provided by the MPC control approach realizes a remarkable result and demonstrates the effectiveness of the MPC technique applied for the ISWEC system.

Command Activity Analysis

Besides power production also other variables are worth to be analysed such as the command activity performed by the designed MPC controller. Command activity analysis allows to understand the energy effort required to realize the MPC command actions and the mechanical stress applied to the gyroscope structure components such as the supporting bearings.

The figure 3.10 illustrates the comparison between the command activity computed during the simulation by MPC controller with the one computed by PD controller when the system is excited by the wave classified as *Wave 1*. The obtained results are analogue for all the other waves, therefore the next observations are valid in general.

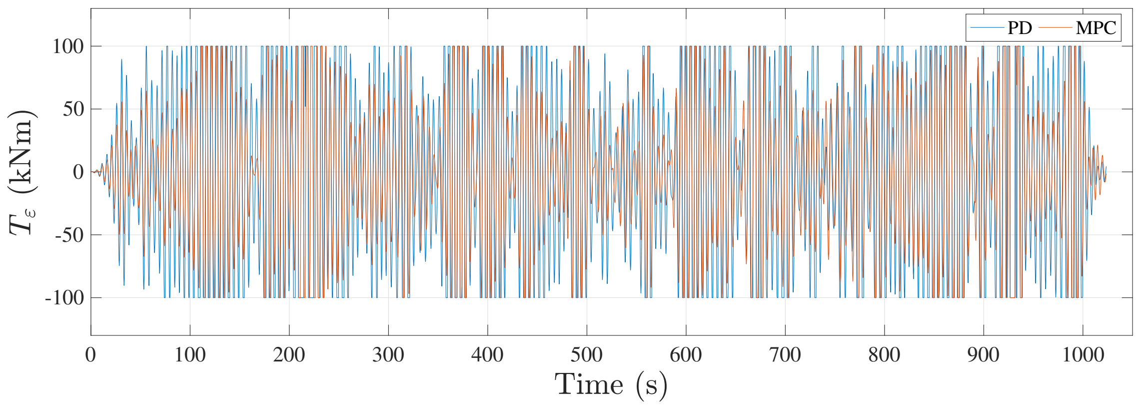

Figure 3.10: Command Activity - PD vs MPC

A first aspect that it is possible to notice is that both controllers provide a command action that satisfies the actuator constraints, which as explained in the the subsection 3.2.2 are given by $\pm 100\,\text{kNm}$. Nevertheless there is an important difference between the PD and MPC constrains fulfilment. As already introduced, the PD controller satisfies the constraints since a saturation of the computed command torque T_ε^{PD} is imposed and performed after its computation. The MPC is instead able to fulfil the constraints limits thanks to the optimization algorithm capability of taking into account the specified bounds in the setting stage and accordingly to provide a command action that results to be the *optimal* and that simultaneously satisfies the imposed constraints.

In figure 3.11 it is shown a section of the previous figure 3.10 in which it is possible to appreciate better the differences between the two command activities. In particular it is possible to observe that despite the MPC control law results to provide a higher produced power than the PD approach, it shows a command activity which is quite softer.

The softer command activity of the MPC with respect to the more aggressive one of the PD provides different benefits to the ISWEC system. A first benefit is related the energy consumption. In particular, as the PTO command torque is provided by actuating an electric motor, giving an higher command action results in a higher energy spent by the electric motor to realize such a command torque. Thus, a lower command action corresponds to reduce energy consumption for actuating the PTO, and therefore it leads to a further improvement in terms of overall energy production.

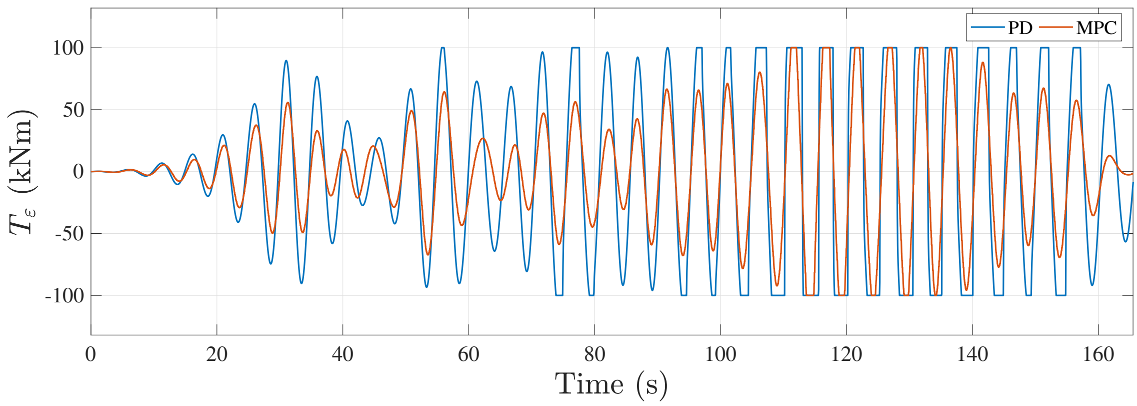

Figure 3.11: Command Activity (section) - PD vs MPC

A second benefit is related to the mechanical stress applied to the gyroscope system, since a softer command activity results is a lower stress for the mechanical components, ensuring a longer lifetime of the components themselves.

For a deeper analysis on the mechanical stress the *RMS* (Root Mean Square) value of the PTO control torque T_ε has been computed, together with the maximum PTO shaft angular speed. The described parameters are computed according to the following definitions:

$$T_{\varepsilon_{RMS}} = \sqrt{\frac{1}{n_s}\sum_{k=1}^{n_s} T_\varepsilon^2(k)}\ , \qquad \dot{\varepsilon}_{max} = \max_k |\dot{\varepsilon}(k)| \tag{3.18}$$

Results of the formulas in (3.18) are shown in figures 3.12 and 3.13 thorough histogram plots.

The figure 3.12 shows the $T_{\varepsilon_{RMS}}$ for the PD in blue and for the MPC in red. It is possible to appreciate that the torque RMS values of the MPC controller are significantly lower than the PD controller ones. This result thus demonstrates how the mechanical structure undergoes to a lower mechanical stress under the MPC control approach.

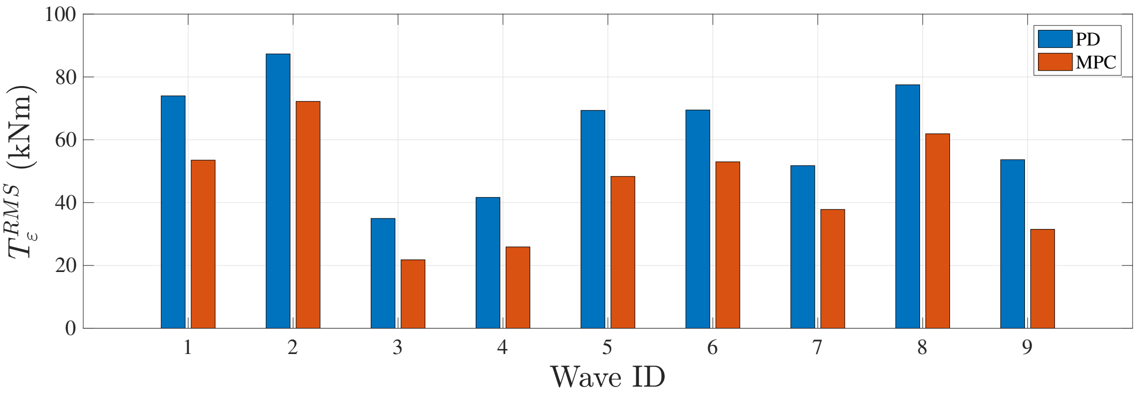

Figure 3.12: RMS Command Torque Histogram

Figure 3.13 shows the maximum angular speed values $\dot{\varepsilon}_{max}$ assumed by the PTO shaft during simulations for the nine waves of interest. The blue values relate to the PD control law whereas the values in red relate to the MPC controller.

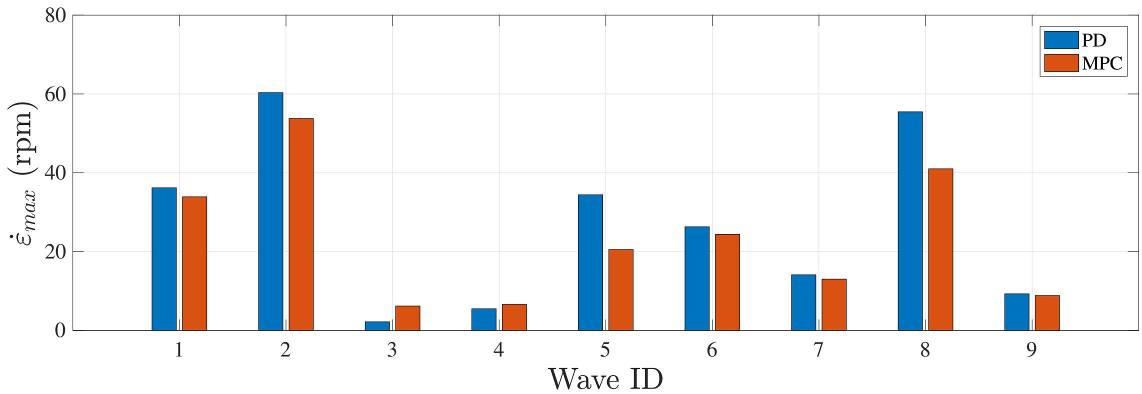

Figure 3.13: Maximum PTO Shaft Angular Speed Histogram

It is possible to see that the MPC approach lets the PTO shaft reach lower values of the PTO maximum speed than the PD approach. The only exceptions refer to the wave profiles *Wave* 3 and *Wave* 4, but this can be considered as an expected behaviour since these two wave profiles are characterized to be quieter with respect to the others (see table 3.2). The quieter behaviour of the sea state lets the ISWEC assume softer dynamics which the MPC control therefore does not minimize as much as the other cases. For this reason the state $\dot{\varepsilon}(k)$ is less damped by the MPC with respect to the other sea states, and therefore the maximum $\dot{\varepsilon}(k)$ results greater than the one assumed under the PD control.

For a quantitative analysis it is possible to evaluate the percentage difference expressed in the formulas in (3.19).

$$\Delta T_{\varepsilon} = \frac{T_{\varepsilon_{RMS}}^{MPC} - T_{\varepsilon_{RMS}}^{PD}}{T_{\varepsilon_{RMS}}^{PD}} \cdot 100\,, \quad \Delta \dot{\varepsilon}_{max} = \frac{\dot{\varepsilon}_{max}^{MPC} - \dot{\varepsilon}_{max}^{PD}}{\dot{\varepsilon}_{max}^{PD}} \cdot 100 \tag{3.19}$$

The results obtained from formulas in (3.19) are reported in table 3.6.

Table 3.6: Command Torque RMS and Maximum PTO Angular Speed - percentage difference between PD and MPC

Wave ID	ΔT_{ε} (%)	$\Delta \dot{\varepsilon}_{max}$ (%)
1	− 27.65	− 6.35
2	− 17.29	− 10.88
3	− 37.65	+ 183.8
4	− 37.82	+ 20.05
5	− 30.30	− 40.36
6	− 23.73	− 7.29
7	− 26.94	− 7.65
8	− 20.12	− 26.07
9	− 41.29	− 4.61

ISWEC States Analysis

It is worth to investigate which is the behaviour assumed by PTO shaft and by the by pitching dynamics of the hull by analysing respectively the states ε, $\dot{\varepsilon}$ and δ, $\dot{\delta}$. The following results relate to a simulation in which the ISWEC model is excited by the wave profile classified as *Wave 1* in table 3.2, but the obtained results are analogue also for the other sea states.

The figure 3.14 shows the time evolution of the state $\varepsilon(t)$, which represents the angular position of the gyroscope system shaft, controlled through the PTO unit with the PD (in blue) and with the MPC approach (in red).

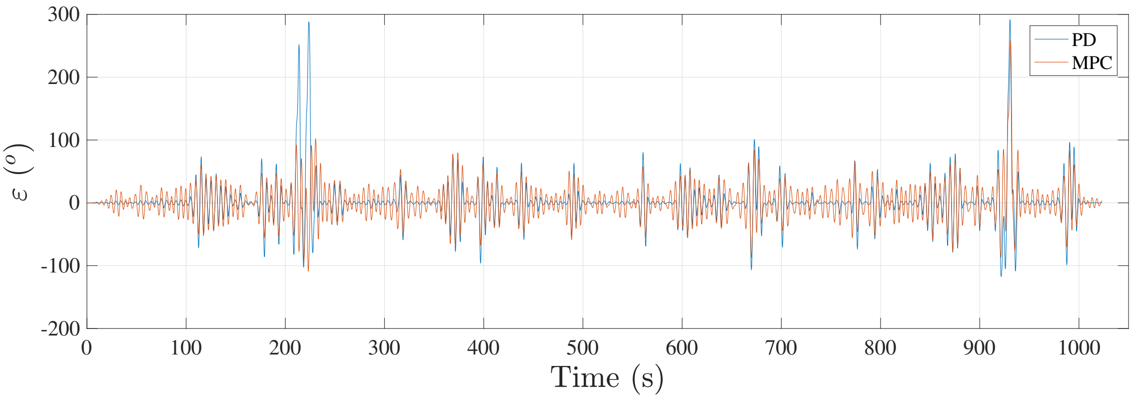

Figure 3.14: PTO shaft angular position - PD vs MPC

A first aspect that it is possible to observe is that the PTO shaft angle $\varepsilon(k)$ oscillates around 0 rad, with both control approaches. Moreover the PTO shaft angle ε never overcome a complete revolution, despite mechanically feasible, which means that $\varepsilon(k)$ is bounded between $\pm 360°$.

The figure 3.15 show a section of figure 3.14 in which it is also reported the wave induced torque $\tau_w(k)$ scaled of $1/10$ in order to be comparable with the other variables.

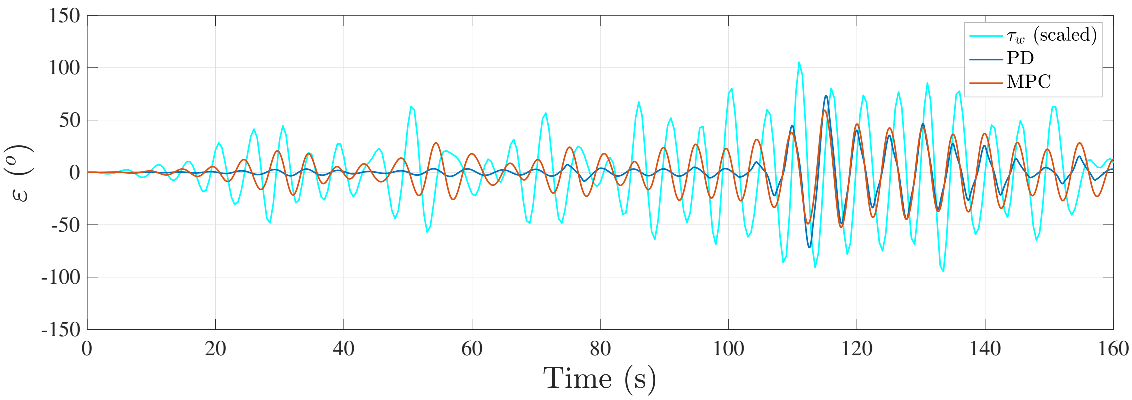

Figure 3.15: PTO shaft angular position (section) - PD vs MPC

The figure 3.15 shows the capability of the MPC to *adapt* to variations of the sea state. In particular focusing on the evolution of the state $\varepsilon(k)$ when the PTO is controlled by the PD it is possible to observe that in first time interval, in which the sea state is quieter, the values assumed by $\varepsilon(k)$ are close 0 rad, which means that the gyroscope is assuming small oscillations, thus producing a low quantity of energy. When the applied torque by the wave $\tau_w(k)$ starts to increase, the state $\varepsilon(k)$ assumes much higher values as well.
The MPC controller, instead, despite the sea state is quiter at the beginning, it allows the gyroscope shaft to move on an higher range with respect to the one related to the PD approach, resulting in an higher produced power (see figure 3.8). When the sea state becomes rougher, which is about after 100 s, the MPC is able to keep the $\varepsilon(k)$ values close to the nominal ones assumed before.
This shaft behaviour provided by the MPC control is achieved by imposing a lower damping through smaller command actions $T_\varepsilon(k)$ when the sea is quieter, and by imposing a stronger damping through higher command actions $T_\varepsilon(k)$ when the sea state is rougher (see figure 3.11).

In figure 3.16 it is possible to evaluate the behaviour of the PTO shaft angular speed $\dot{\varepsilon}(k)$. As already introduced it is important to investigate the state $\dot{\varepsilon}(k)$ as if PTO shaft angular speed exceeds a certain threshold it could be dangerous for the electronic devices connected to the PTO unit. In the figure it is possible to observe that both control approaches satisfy the limit for the $\dot{\varepsilon}(k)$ which as discussed in chapter 2 results to be ± 50 rpm.

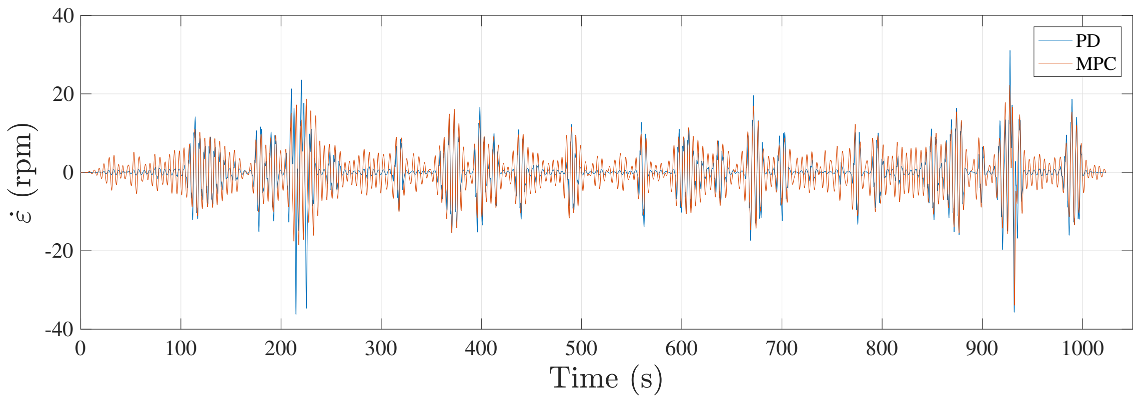

Figure 3.16: PTO shaft angular speed (Wave 1) - PD vs MPC

As far as the $\dot{\varepsilon}(k)$ state bounds are concerned it is relevant to investigate the behaviour shown by this state in the critical case, which as reported in the histogram 3.13 results to occur under the excitation of the wave profile *Wave 2*. To this end the figure 3.17 shows the time evolution of the state $\dot{\varepsilon}(k)$ when the system is excited by *Wave 2*. The dashed black lines in the figure illustrate the bounds of ± 50 rpm.

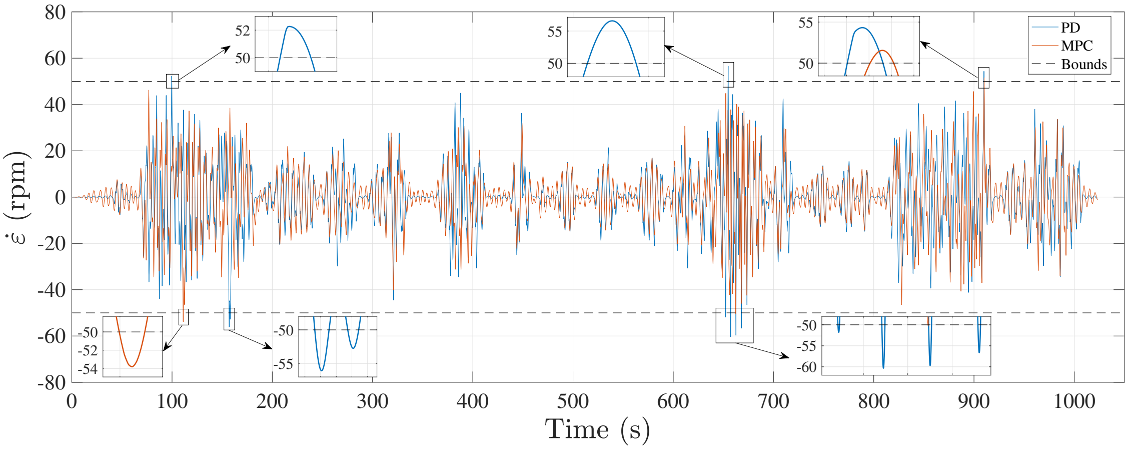

Figure 3.17: PTO shaft angular speed (Wave 2) - PD vs MPC

In particular in figure 3.17 it is possible to see that the PD controller allows the state $\dot{\varepsilon}(t)$ overcome the bounds several times and of a significant extent. The MPC controller, instead, is able to keep the evolution of $\dot{\varepsilon}(k)$ to lower values allowing it to reach the bounds only in two cases and of a negligible extent. This makes the MPC controller safer for the PTO unit with respect to the PD.

As far as the state $\dot{\varepsilon}(k)$ is concerned it is possible to make another consideration. To this end in figure 3.18 it is reported a section of figure 3.16 in which it also reported the time evolution of the applied torque by the wave τ_w scaled of 1/50 in order to be comparable with the other variables. As it has been seen for the state $\varepsilon(t)$, in this figure it is possible to observe the capability of the *MPC controller* to adapt the state $\dot{\varepsilon}(k)$ dynamics according to the sea state variations. In particular it is possible to see the capability of the MPC controller of letting the shaft angular speed assume a quite regular behaviour. This means that the shaft angular speed reaches almost the same peaks values independently from the sea state. The case is different for the PD controller which instead makes the state $\dot{\varepsilon}(t)$ assume much lower peaks in quiet sea state conditions, resulting therefore in a low produced power (see figure 3.8).

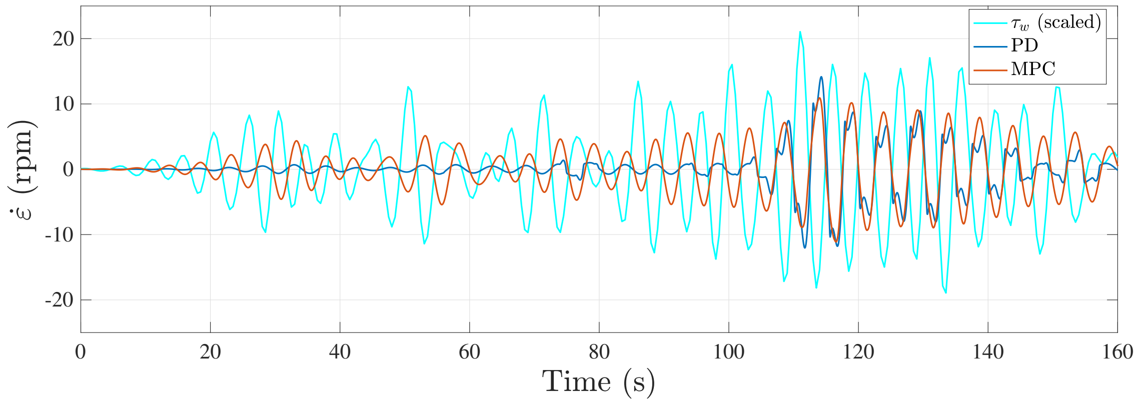

Figure 3.18: PTO shaft angular speed (section) - PD vs MPC

As discussed for the state $\varepsilon(k)$ the capability of the MPC controller do adapt the state $\dot{\varepsilon}(k)$ to the sea state variations relies in the optimization algorithm which adapts the computed command torque basing on the cost function value, which depends on the measured states. The result is therefore a softer damping in quiet sea states and a stronger damping in rougher sea states (see figure 3.11).

It is interesting to analyse the behaviour of the states $\delta(k)$ and $\dot{\delta}(k)$ as they represent the angular position assumed by the hull and its the angular speed respectively.

The figure 3.19 shows the time evolution behaviour of the state $\delta(k)$ comparing the PD shown by the blue line with the MPC shown by the red line.

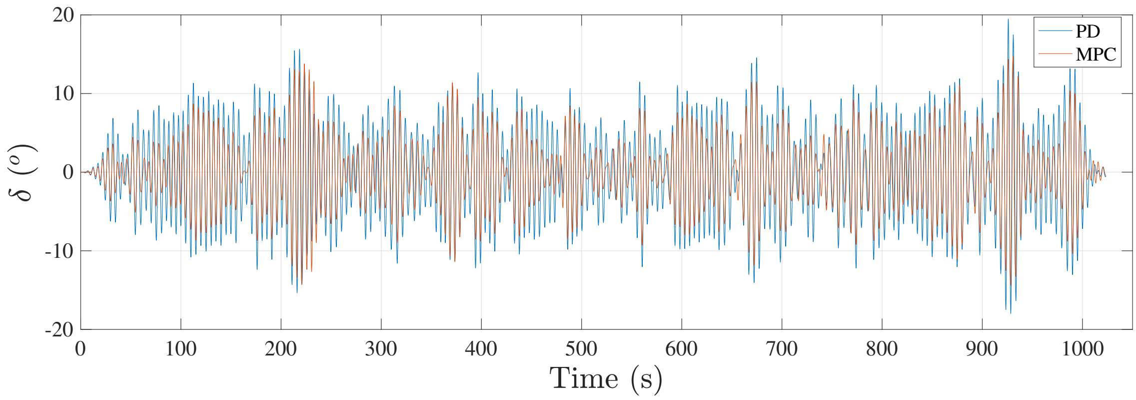

Figure 3.19: Hull angular position - PD vs MPC

In figure 3.19 it is possible to notice that for both the controller approaches the rotation of the hull about δ-axis is bounded between $\pm 20°$, where the linear approximation of the Cummins' equation can be considered valid, as described in [11]. Moreover the figure shows how the behaviour of $\delta(k)$ assumes lower peak values under the MPC control with respect to the PD case. This means that the oscillations of the hull are characterized by lower pitch inclination under the MPC control and thus the approximation provided by the linearized model results to be more accurate.

The figure 3.20 shows the time evolution of the hull angular velocity $\dot{\delta}(k)$.

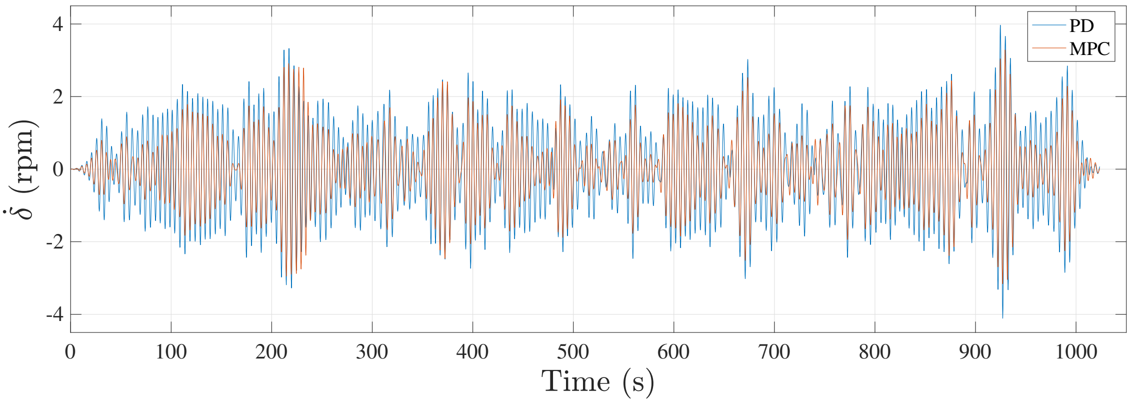

Figure 3.20: Hull angular speed - PD vs MPC

In this figure it is possible to see that also the behaviour of the state $\dot{\delta}(k)$ is characterized by lower peak values under the control of the MPC with respect to the PD case. This means that the oscillating behaviour of the hull oscillates with slower angular pitch velocity with respect to the PD case. This demonstrates that the approximation discussed in chapter 2 about the linearization of the dynamic equations results to be valid. In particular defining the maximum value of pitch angular speed as

$$\dot{\delta}_{max} = \max_{k} |\dot{\delta}(k)| \tag{3.20}$$

it is possible to analyse the maximum values assumed by the state $\dot{\delta}(k)$ during the simulations. The table 3.7 summarizes the result of formula (3.20) for the nine wave profiles.

Table 3.7: Hull Maximum Pitch Speeds

Wave ID	$\dot{\delta}_{max}$ $(rad\, s^{-1})$
1	0.34
2	1.1
3	0.11
4	0.12
5	0.29
6	0.24
7	0.21
8	0.59
9	0.17

3.3 Augmented MPC for ISWEC

This subsection addresses the *augmented MPC* controller for the ISWEC system, which consists of an upgraded version of the previously designed MPC and it characterized by the adoption an *augmented model* as prediction model. The augmented model allows to take into account the contribution of the induced torque by the wave $\tau_w(k)$ into the dynamics prediction, despite in a simplified form, leading to a more accurate prediction of the system dynamics. The following subsections describe the system architecture, the simulink model, the control problem, the implementation and the provided results.

3.3.1 Control System Architecture

The figure 3.21 shows the architecture of the ISWEC system with the *augmented MPC* controller.

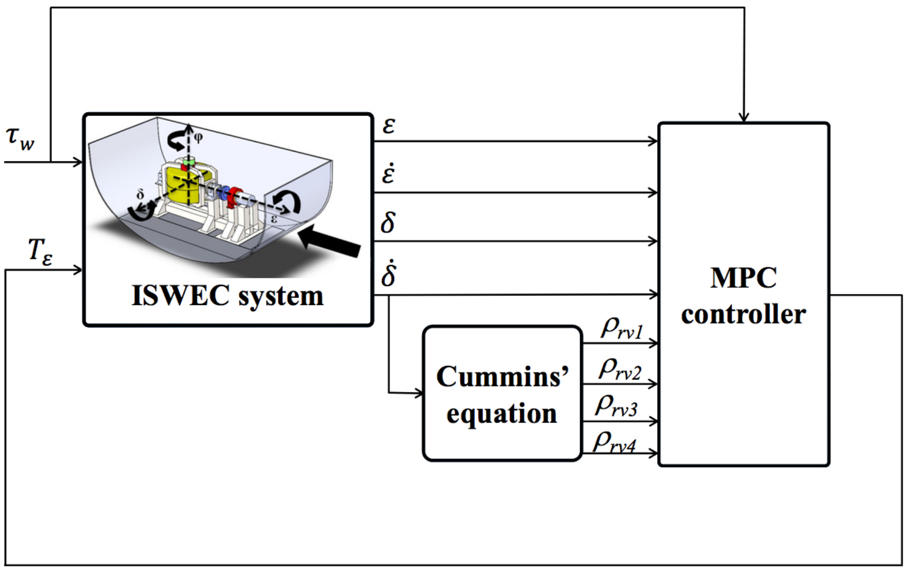

Figure 3.21: Control System Architecture - Augmented MPC

In the shown architecture it is possible to observe that the induced torque τ_w besides entering the ISWEC system it also enters in the MPC controller. The measure of τ_w is required by the augmented model of the MPC controller in order to be used together with the measure of the states for providing a more accurate prediction and therefore a more accurate command action.

In figure 3.22 it is shown the Simulink model of the system architecture presented in figure 3.21. The meaning of the signals and the blocks have been already discussed in the standard MPC control in section 3.2. In this model it's possible to observe that besides the states the *CONTROLLER* subsystem takes an additional variable, that is the wave forces signal F_w, which includes the τ_w value required by the MPC. The signal τ_w is therefore selected from F_w inside the *CONTROLLER* subsystem as shown in figure 3.23.

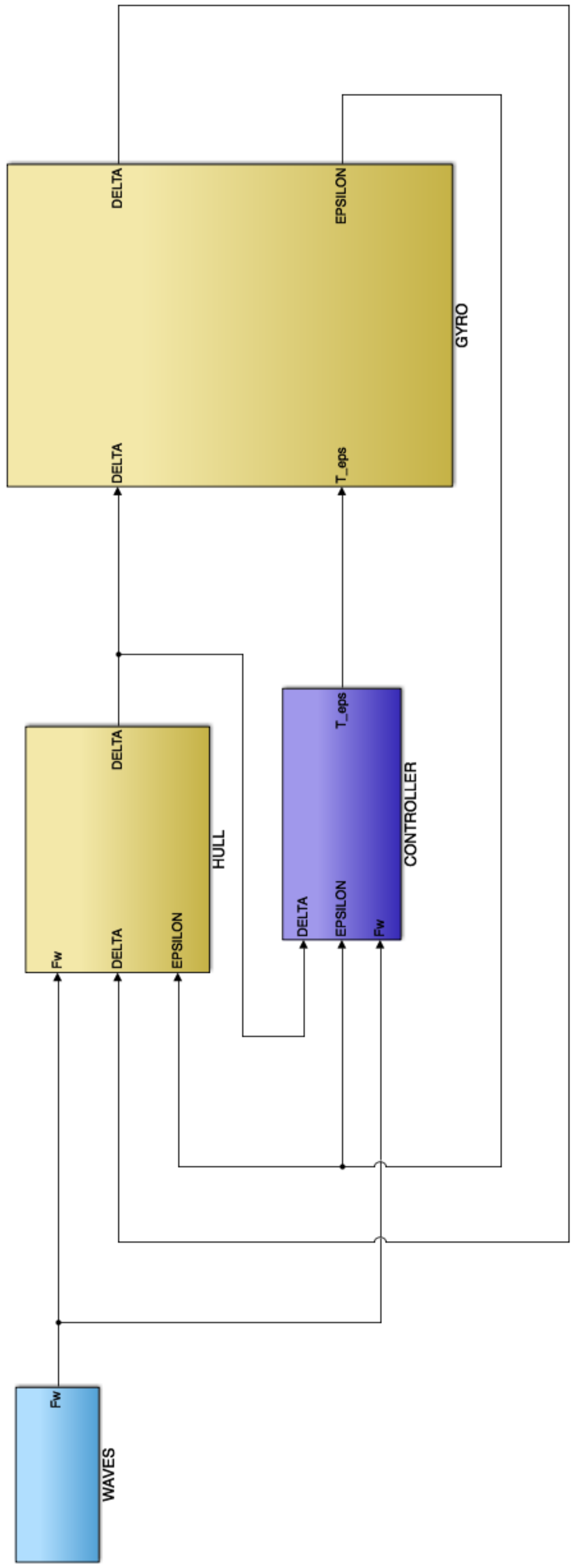

Figure 3.22: Simulink Model - Augmented MPC

The figure 3.23 shows the *CONTROLLER* subsystem. It is possible to observe that the *MPC controller* takes, besides the states provided by the *Full State Builder* subsystem discussed in section 3.2, also the measure of τ_w selected through a *selector* block from the signal F_w. Despite the variable τ_w evolves as a continuous-time signal the MPC controller samples its measure at each sampling time T_s and keeps it constant till the next sampling instant.

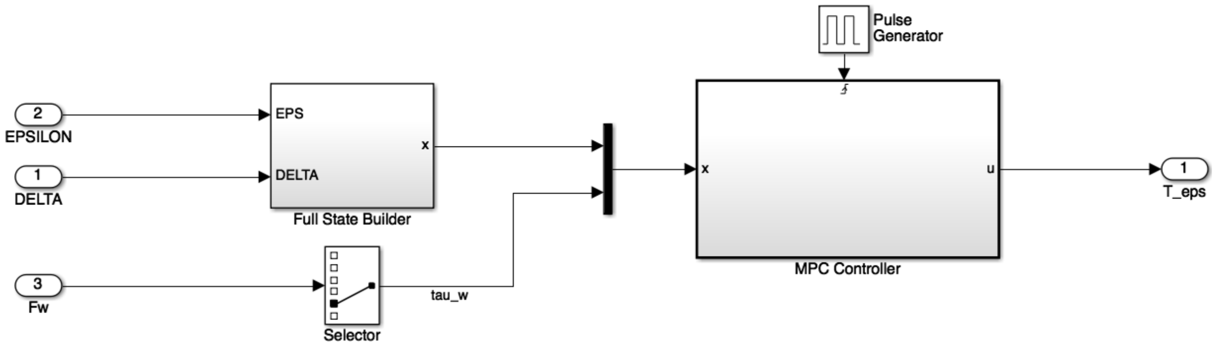

Figure 3.23: Controller Subsystem - Augmented MPC

3.3.2 Augmented MPC control problem

As already introduced the *augmented MPC* consists of un upgraded version of the previously designed MPC which is characterized by the adoption of an *augmented model* as prediction model. This strategy allows the MPC controller to perform a more accurate prediction, resulting therefore in a more accurate command action T_ε which is suited to the more realistic computed prediction.

In particular, the discrete-time *prediction model* used in this approach by MPC controller is defined as:

$$\boldsymbol{x}_{aug}(k+1) = \boldsymbol{A}_{aug}\, \boldsymbol{x}_{aug}(k) + \boldsymbol{B}_{aug}\, u(k) \tag{3.21}$$

The state vector is now $\boldsymbol{x}_{aug}(k) \in \mathbb{R}^9$ since it contains the the additional state $\tau_w(k)$, indicating the applied torque on the hull by the wave about the pitch axis. As already introduced the additional state $\tau_w(k)$ represents a *disturbance* for the MPC prediction model since it is a not manipulable input, and for this reason it is referred to as $d(k)$. The state $\boldsymbol{x}_{aug}(k)$ measured by the MPC controller is defined as

$$\boldsymbol{x}_{aug} = \begin{bmatrix} \dot{\varepsilon}(k) & \varepsilon(k) & \dot{\delta}(k) & \delta(k) & \rho_{rv,1}(k) & \rho_{rv,2}(k) & \rho_{rv,3}(k) & \rho_{rv,4}(k) & d(k) \end{bmatrix}^T \tag{3.22}$$

As far as the prediction model (3.21) is concerned, the *state matrix* $\boldsymbol{A}_{aug}$ and the the *input matrix* $\boldsymbol{B}_{aug}$ are computed through a series of operations hereafter presented.

Besides the *state matrix* $\boldsymbol{A}$ and the *input matrix* $\boldsymbol{B}$ already used in the standard MPC controller in section 3.2 the augmented model makes use also of the *disturbance input matrix* $\boldsymbol{B}_d$ related to the induced torque by the forcing wave.

$$\boldsymbol{B}_d = \begin{bmatrix} 0 & 0 & \dfrac{1}{I_{eq}} & 0 & 0 & 0 & 0 & 0 & 0 \end{bmatrix}^T \tag{3.23}$$

The continuous-time model that has to be discretized is defined as:

$$\dot{\boldsymbol{x}}(t) = \boldsymbol{A}\,\boldsymbol{x}(t) + \tilde{\boldsymbol{B}}\,u(t) \tag{3.24}$$

where:

$$\tilde{\boldsymbol{B}} = \begin{bmatrix} \boldsymbol{B} & \boldsymbol{B}_d \end{bmatrix} \in \mathbb{R}^{8\times 2} \tag{3.25}$$

The construction of the matrix $\tilde{\boldsymbol{B}}$ is required to obtain from the discretiazion operation both the discretized *input matrix* and discretized *disturbance input matrix* respectively called $\boldsymbol{B}_{DT}$ and $\boldsymbol{B}_{d_{DT}}$, shown in (3.26).

Calling the result of the discretized matrix $\boldsymbol{A}$ as $\boldsymbol{A}_{DT}$ and calling the result of the discretized matrix $\tilde{\boldsymbol{B}}$ as $\tilde{\boldsymbol{B}}_{DT}$, where:

$$\tilde{\boldsymbol{B}}_{DT} = \begin{bmatrix} \boldsymbol{B}_{DT} & \boldsymbol{B}_{d_{DT}} \end{bmatrix} \tag{3.26}$$

the augmented model matrices are built as follows:

$$\boldsymbol{A}_{aug} = \begin{bmatrix} \boldsymbol{A}_{DT} & \boldsymbol{B}_{d_{DT}} \\ \boldsymbol{0} & 1 \end{bmatrix} \tag{3.27}$$

$$\boldsymbol{B}_{aug} = \begin{bmatrix} \boldsymbol{B}_{DT} & 0 \end{bmatrix}^T \tag{3.28}$$

Where:

- $\boldsymbol{A}_{DT} \in \mathbb{R}^{8\times 8}$;
- $\boldsymbol{B}_{d_{DT}} \in \mathbb{R}^{8\times 1}$;
- $\boldsymbol{0} \in \mathbb{R}^{1\times 8}$;
- $1 \in \mathbb{R}$;
- $\boldsymbol{B}_{DT} \in \mathbb{R}^{8\times 1}$;
- $0 \in \mathbb{R}$.

It is worth to notice how the augmented model includes the disturbance in the dynamics. In particular, substituting the matrices (3.27) and (3.28) into the discrete-time model defined in (3.21) adopting the state vector presented in (3.22) it is possible to obtain the dynamic evolution of the state $d(k)$, which results to be

$$d(k+1) = d(k)$$

This means that the value of induced torque $\tau_w(k)$ sampled by the MPC controller in the current instant k is kept constant for all the prediction horizon in the dynamics prediction, even though it actually changes values in the future time steps. Therefore the augmented model accounts for the wave contribution in a simplified fashion.

3.3.3 Implementation

As well as the *standard MPC* also the *augmented MPC* control problem has been implemented making use of the toolboxes MPT3 and YALMIP, with the same purposes. Therefore, the former is used for setting up all the MPC problem whereas the latter is used for customizing the *cost function*. The difference lies in the *prediction model* set in the MPC controller. In particular, the *augmented model* has been implemented according to the procedure discussed in the previous subsection and then has been set as prediction model through the MPT3 toolbox. Consequently, as for the standard MPC implementation, the MPC object has been created in MATLAB environment and used for simulations in Simulink environment.

Simulations of the ISWEC nonlinear model controlled by the augmented MPC results to achieve the optimal tradeoff adopting for the paramters the same tuning used for the standard MPC controller. The parameters list and their tuned values are reported in table 3.8.

Table 3.8: Augmented MPC parameters

Parameter	**Value**	**Description**
T_s	50 ms	Sampling Time
H_p	2	Prediction Horizon
q_{11}	$1 \cdot 10^9$	Q matrix weight
q_{22}	$3 \cdot 10^{10}$	Q matrix weight
n_1	1	N matrix weight
r	0.020	R matrix Weight
$T_{\varepsilon_{max}}$	$+100\,(\text{kNm})$	Constraint
$T_{\varepsilon_{min}}$	$-100\,(\text{kNm})$	Constraint

3.3.4 Results

This subsection discusses the results obtained adopting the designed *augmented MPC* controller during simulations of the ISWEC nonlinear model. The results focus on the produced power only, as the dynamics of the states and the command activity behaviour results to be analogue to the ones already observed in the standard MPC controller resulting thus in the same observations and improvements already discussed.

In figure 3.24 it is reported the *absorbed power* trend obtained with MPC approach in blue and the augmented MPC approach in red.

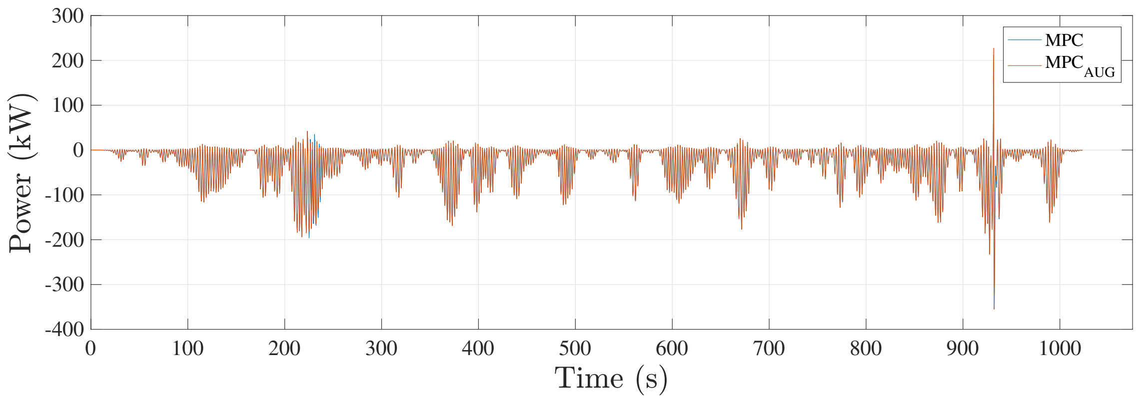

Figure 3.24: Absorbed Power Plot - MPC vs Augmented MPC

In figure 3.24 it appears that the absorbed power trend provided by the two MPC approaches is identical but they actually differ slightly each other, as shown in figure 3.25 in which is reported a section of the figure 3.24 and a magnified portion of the plot showing the peaks difference between the two different control approaches.

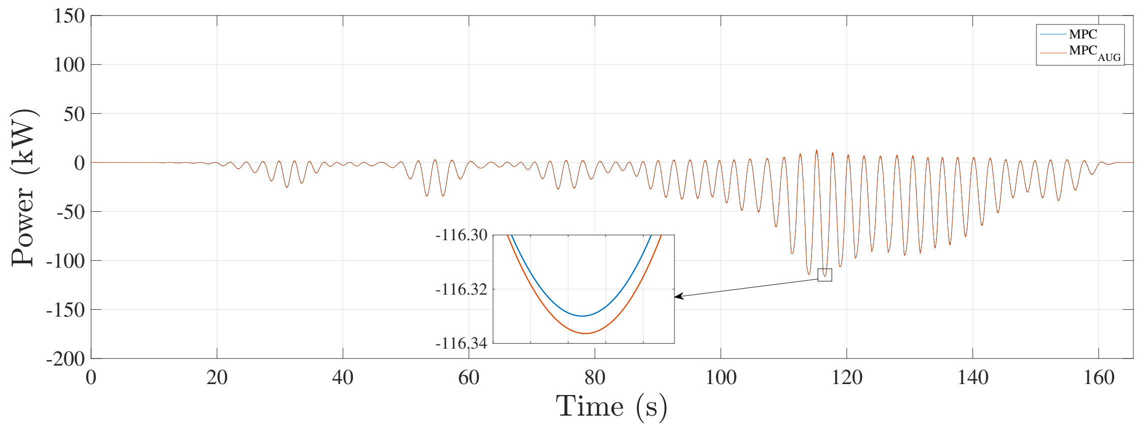

Figure 3.25: Absorbed Power Plot (section) - MPC vs Augmented MPC

Thus, the figure 3.25 shows the capability of the augmented MPC controller to provide an improved result since an higher negative peak indicates an higher produced power, as already discussed.

For a quantitative analysis it is possible to compute the *produced mean power* according to the following formula already introduced and discussed, hereafter reported.

$$\overline{P} = -\frac{1}{n_s}\sum_{k=1}^{n_s} P(k)$$

Starting from the obtained values of $\overline{P}$ it is again possible to compute the normalized produced mean power $\widehat{P}$ defined as

$$\widehat{P} = \frac{\overline{P}}{\overline{P}_{max}}$$

where $\overline{P}_{max}$ is the maximum *produced mean power* among *MPC* and *augmented MPC* results.

The *normalized produced mean power* results are summarized in the table 3.9, in which each row reports the identification of the wave profile used in the simulation and the corresponding normalized produced mean power with the *MPC* approach and the *augmented MPC* approach respectively referred to as $\widehat{P}^{std}_{MPC}$ and $\widehat{P}^{aug}_{MPC}$.

Table 3.9: Normalized Produced Mean Power - Augmented MPC

Wave ID	$\widehat{P}^{std}_{MPC}$	$\widehat{P}^{aug}_{MPC}$
1	0.42408	0.42552
2	1.00	0.99924
3	0.05643	0.05644
4	0.08122	0.08125
5	0.31046	0.31055
6	0.37492	0.37491
7	0.16716	0.16717
8	0.57373	0.57684
9	0.12673	0.12678

The results reported in table 3.9 demonstrate that the augmented MPC approach provides a slight improvement with respect to standard MPC approach. In particular with exception of the wave profiles Wave 2 and Wave 6 the MPC approach generates an higher produced power.

For a more detailed analysis it is worth to evaluate the percentage difference between the power produced by the two MPC control approaches, according to the formula

$$\Delta\overline{P}_{MPC} = \frac{\overline{P}^{aug}_{MPC} - \overline{P}^{std}_{MPC}}{\overline{P}^{std}_{MPC}} \cdot 100 \tag{3.29}$$

Results of the formula 3.29 are reported in table 3.10.

Table 3.10: Produced Power percentage increment - Augmented MPC

Wave ID	$\Delta \overline{P}_{MPC}$ (%)
1	$+0.339$
2	-0.076
3	$+0.027$
4	$+0.035$
5	$+0.027$
6	-0.002
7	$+0.009$
8	$+0.542$
9	$+0.040$

In order to evaluate the effective improvement it is possible to compute the yearly energy production according to the formula (3.17) already introduced. The results of this formula have been reported in table 3.11, which summarizes the yearly energy production provided by the standard *MPC* approach and the *augmented MPC* approach respectively referred to as E_{year}^{MPC} and $E_{year}^{MPC(AUG)}$

Table 3.11: Normalized Yearly Energy Production - Augmented MPC

$\widehat{E}_{year}^{MPC}$	$\widehat{E}_{year}^{MPC(AUG)}$
0.998	1.00

Finally, it is possible to evaluate the percentage difference of the yearly energy production between the two different MPC control approaches according to the definition

$$\Delta E_{year}^{MPC(AUG)} = \frac{E_{year}^{MPC(AUG)} - E_{year}^{MPC}}{E_{year}^{MPC}} \cdot 100$$

which provides

$$\Delta E_{year}^{MPC(AUG)} = 0.1058\,\%$$

Thus, the *augmented MPC* results to provide a further improvement to the energy production with respect the previously designed MPC, which consists of an energy increment of about 0.10 %.

3.4 MPC with Known Disturbance for ISWEC

This subsection addresses the *MPC with known disturbance* control problem, which consists of an upgraded version of the previously designed *augmented MPC*. The improvement consists in providing the MPC controller with the feature of performing a prediction of the system dynamic by considering the *real future values* assumed by the wave induced torque $\tau_w(k)$. The sequence of values assumed by the induced torque $\tau_w(k)$ from the current instant k till the H_p^{th} step ahead is assumed to be known a priori at each sampling time.

3.4.1 Control System Architecture

The figure 3.26 shows the architecture of the ISWEC system with the *MPC with known disturbance* controller.

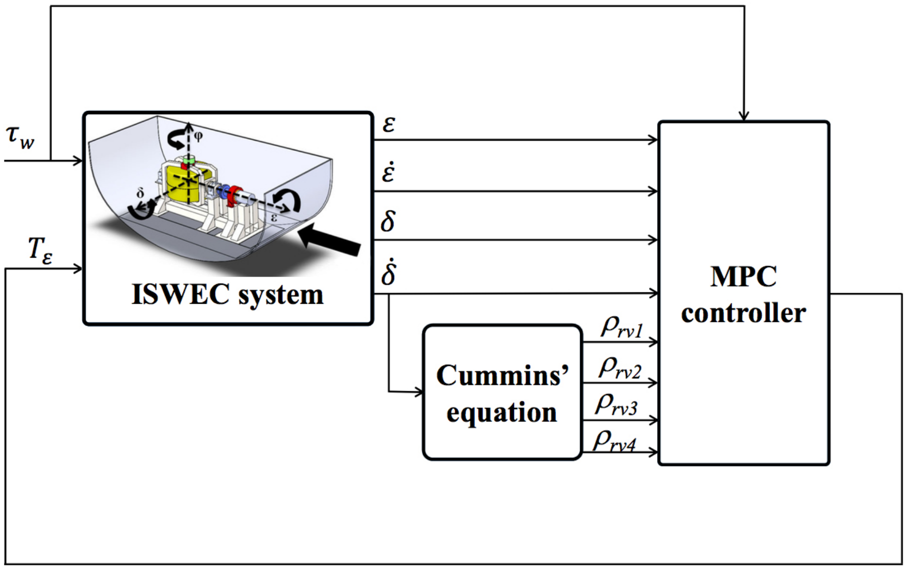

Figure 3.26: Control System Architecture - MPC with Known Disturbance

The architecture configuration is identical to the one discussed for the *augmented MPC*, but the difference lies in the signal τ_w entering in the MPC controller. In this case the signal τ_w consists of a sequence of values which implement the measures of the induced torque by the wave, from the current instant k until the H_p^{th} step ahead, as defined in the following vector

$$\tau_w = \left[\tau_w(k), \quad \tau_w(k+1), \quad \dots, \quad \tau_w(k+Hp)\right] \tag{3.30}$$

As far as the ISWEC system block is concerned despite the vector 3.30 is available, at each sampling time k only the first sample is supposed to excite the system, i.e. $\tau_w(k)$.

The Simulink model implementing the discussed architecture is reported in figure 3.27 as a full page image for a clear visualization.

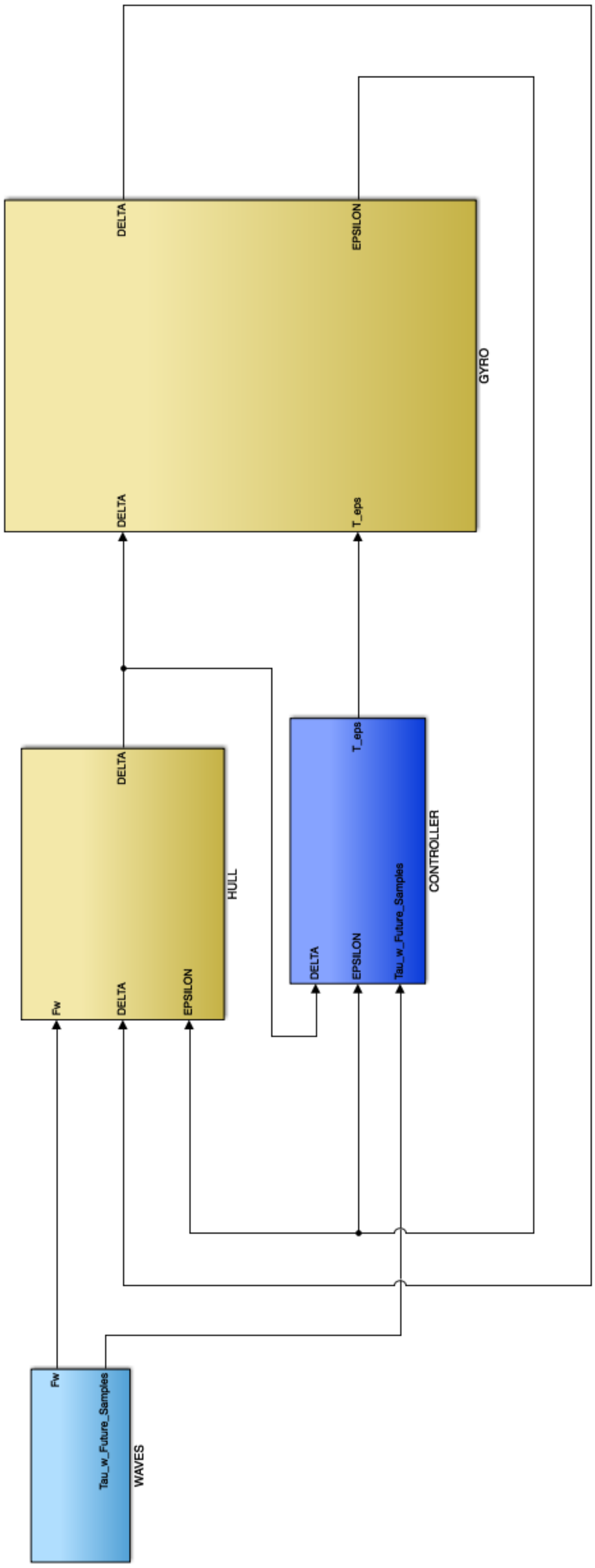

Figure 3.27: Simulink Model - MPC with Known Disturbance

In the Simulink model in figure 3.27 it is possible to notice that the subsystem *WAVES* provides two signals. One of these is τ_w, who is the induced torque already discussed in the previous MPC versions, and *Tau_w_Future_Samples* which is the new signal that implements the sequence defined in (3.30). The signal *Tau_w_Future_Samples* is therefore fed to the MPC controller that will use the contained measures for predicting in accurate way the evolution of the system dynamics.

The figure 3.28 illustrates the subsystem *CONTROLLER* of the Simulink model in figure 3.27.

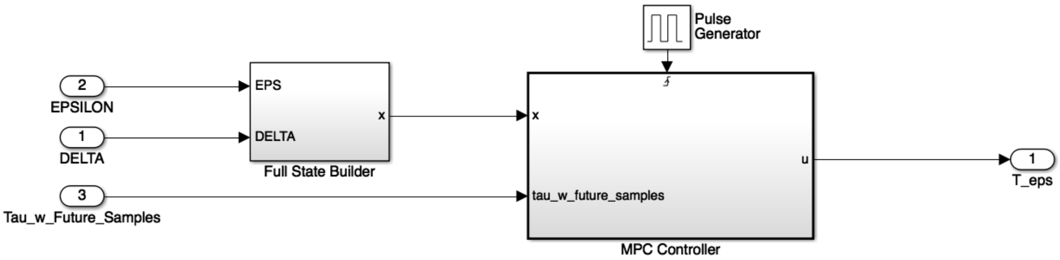

Figure 3.28: Controller Subsystem - MPC with Known Disturbance

It is worth to notice that the variable called *Tau_w_Future_Samples* is not added to the state $\boldsymbol{x}(k)$ through a multiplexer as happens for the *augmented MPC* version but enters in the *MPC Controller* as different variable.

3.4.2 MPC with Known Disturbance control problem

The idea behind *MPC with known disturbance* control problem is to perform accurate predictions of the system dynamics including in the prediction the wave contribution knowing its future behaviour. In the previously designed *augmented MPC* controller it is sufficient to know the current measure $\tau_w(k)$ as it is kept constant for all the prediction horizon, leading to an approximate prediction. In the *MPC with known disturbance* it is necessary to know also and future measures of induced torque besides the current one, as defined in (3.30), which are used to perform an accurate prediction.

The MPC controller capability to provide an accurate prediction is realized through the adoption of a more sophisticated prediction model, which computes the system dynamics prediction basing on the *state* $x(k)$, *input* $u(k)$ and *disturbance* $d(k)$ dynamics. The *prediction model* is defined as

$$\boldsymbol{x}(k+1) = \boldsymbol{A}_{DT}\, \boldsymbol{x}(k) + \boldsymbol{B}_{DT}\, u(k) + \boldsymbol{B}_{d_{DT}}\, d(k) \tag{3.31}$$

where

- $\boldsymbol{x}(k) = \begin{bmatrix} \dot{\varepsilon}(k) & \varepsilon(k) & \dot{\delta}(k) & \delta(k) & \rho_{rv,1}(k) & \rho_{rv,2}(k) & \rho_{rv,3}(k) & \rho_{rv,4}(k) \end{bmatrix}^T \in \mathbb{R}^{8\times 1}$ is the state;
- $u(k) \in \mathbb{R}$ is the manipulable input and corresponds to the command torque $T_\varepsilon(k)$;
- $d(k) \in \mathbb{R}$ is the disturbance and corresponds to the measure of $\tau_w(k)$.

The *state matrix* $\boldsymbol{A}_{DT}$, the *input matrix* $\boldsymbol{B}_{DT}$ and the *disturbance input matrix* $\boldsymbol{B}_{d_{DT}}$ are obtained from the discretization process already discussed in the *augmented MPC* control problem in section 3.3, but in the current context these matrices are explicitly used in the model (3.31), and not for developing the augmented model.

3.4.3 Implementation

The implementation of the *MPC with known disturbance* control problem takes place completely through YALMIP toolbox in this case. This choice is required since the MPT3 toolbox, used for setting up the problem in the other cases, does not allow to set a *prediction model* that involves also a *disturbace* term besides the *states* and the *input* of the system, as the one in (3.31).

Despite YALMIP adopts a different method for defining an MPC control problem, it allows through a series of operation to create an *MPC object* as well as the MPT3 toolbox does. The created MPC object, thus, gives the the chance to call the optimization *function* which takes the required data in input and provides the *optimal* control action $T_\varepsilon(k)$ as output. This function is called by the *MPC Controller* shown in figure 3.28 at each sampling time k.

The data required by the optimization function which must be available at each sampling time k are the following:

- $\boldsymbol{x}(k)$;
- $\big[d(k), \quad d(k+1), \quad \dots, \quad d(k+H_p)\big]$.

The optimal tuning of MPC parameters which result to provide the optimal tradeoff maximizing the produced power corresponds to the tuning adopted for the other two control approaches, summarized in table 3.12.

Table 3.12: Parameters of MPC with Known Disturbance

Parameter	**Value**	**Description**
T_s	50 ms	Sampling Time
H_p	2	Prediction Horizon
q_{11}	$1 \cdot 10^9$	Q matrix weight
q_{22}	$3 \cdot 10^{10}$	Q matrix weight
n_1	1	N matrix weight
r	0.020	R matrix Weight
$T_{\varepsilon_{max}}$	$+100$ (kNm)	Constraint
$T_{\varepsilon_{min}}$	-100 (kNm)	Constraint

3.4.4 Results

This subsection shows the results obtained by the *MPC with known disturbance* controller during the simulation of the nonlinear ISWEC model for the nine wave profiles of interest (in table 3.2). Produced power results only are shown as the states dynamics and the command activity result to be analogue to the the standard MPC approach, resulting thus in the same observations.

In figure 3.29 it is reported the *absorbed power* trend obtained with *augmented MPC* approach in red and the *MPC with known disturbance* approach in green.

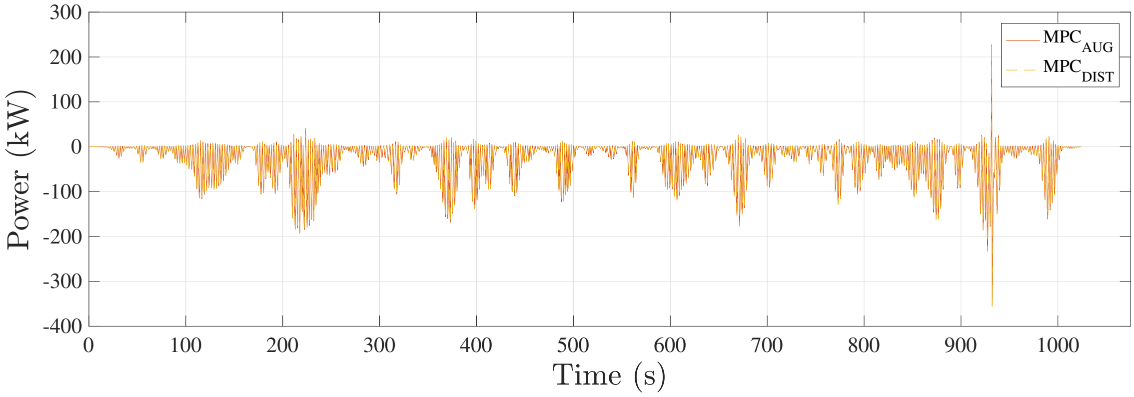

Figure 3.29: Absorbed Power Plot - Augmented MPC vs MPC with Known Disturbance

It is possible to observe that the two absorbed power trends result to be identical. For a closer view it is possible to observe the figure 3.30 which reports a section of the figure 3.29 in which is also illustrated a magnified portion of the plot containing the peak comparison between the *augmented MPC* and the *MPC with known disturbance*.

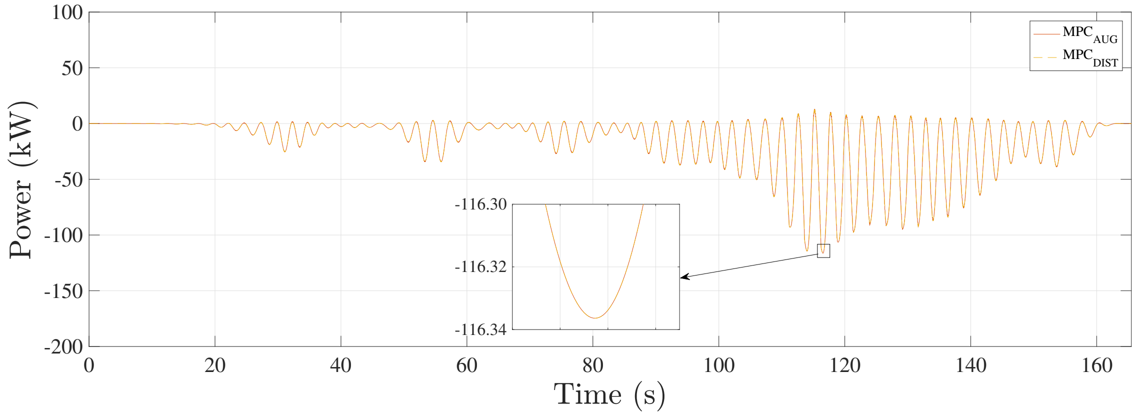

Figure 3.30: Absorbed Power Plot (section) - Augmented MPC vs MPC with Known Disturbance

From the figures 3.29 and 3.30 it is observable that the two MPC control approaches result to provide the same absorbed power trend.

For a quantitative evaluation the *produced mean power* has been computed according to the already discussed following formula

$$\overline{P} = -\frac{1}{n_s}\sum_{k=1}^{n_s} P(k)$$

Having the values of $\overline{P}$ it is possible to compute the normalized produced mean power as

$$\widehat{P} = \frac{\overline{P}}{\overline{P}_{max}}$$

where $\overline{P}_{max}$ is the maximum produced mean power among the results obtained by *MPC*, *augmented MPC* and *MPC with known disturbance*.

Results of the normalized produced mean power are reported in table 3.13, where each row reports the wave identification and the normalized produced mean power by the three different MPC approaches. $\widehat{P}^{std}_{MPC}$, $\widehat{P}^{aug}_{MPC}$ and $\widehat{P}^{dist}_{MPC}$ denote respectively the results obtained with the *standard MPC*, *augmented MPC* and the *MPC with known disturbance*.

Table 3.13: Normalized Produced Mean Power - MPC with Known Disturbance

Wave ID	$\widehat{P}^{std}_{MPC}$	$\widehat{P}^{aug}_{MPC}$	$\widehat{P}^{dist}_{MPC}$
1	0.42408	0.42552	0.42552
2	1.00	0.99924	0.99924
3	0.05643	0.05644	0.05644
4	0.08122	0.08125	0.08125
5	0.31046	0.31055	0.31055
6	0.37492	0.37491	0.37491
7	0.16716	0.16717	0.16717
8	0.57373	0.57684	0.57684
9	0.12673	0.12678	0.12678

Also from the quantitative point of view the produced mean power obtained with the *MPC with known disturbance* approach results to be identical to the one provided by the *augmented MPC*.

The reason why the produced mean power results to be the same for both the *augmented MPC* and the *MPC with known disturbance* lies in the *prediction horizon* H_p. In particular, the tuning of the parameters which allows to obtain the optimal tradeoff between states behaviour, command activity and maximization of the produced power provides for a prediction horizon set to $H_p = 2$ (see table 3.12), whose value results to be not long enough for allowing differences between the *augmented MPC* and the *MPC with kwown disturbance*. Thus, predicting the state evolution of only 2 steps in the future is such that the wave contribution included into the dynamics prediction by the *MPC with known disturbance* approach has the same effect as the one provided by the *augmented MPC* approach.
Therefore, in order to observe different results between the *MPC with known disturbance* and the *augmented MPC* it is necessary to set the prediction horizon H_p to a value sufficiently long. As an example the table 3.14 reports the normalized produced mean power obtained considering the *Wave 1* with a prediction horizon set as $H_p = 20$.

Table 3.14: Normalized Produced Mean Power - MPC with Known Disturbance ($H_p = 20$)

Wave ID	$\widehat{P}^{std}_{MPC}$	$\widehat{P}^{aug}_{MPC}$	$\widehat{P}^{dist}_{MPC}$
1	0.990	0.997	1.00

The results reported in table 3.14 show that the *MPC with known disturbance* is able to produce a greater power than the *augmented MPC* provided that the prediction horizon is sufficiently long. It is worth to remark that the three normalized produced mean power values in table 3.14 refer to absolute produced mean power values which are lower than the optimal case reported in table 3.13, as in this last case the value of H_p is not the optimal one.

In figure 3.31 it is shown the absorbed power trend by the three different MPC approaches with a prediction horizon set as $H_p = 20$, when ISWEC nonlinear model is excited by the input wave classified as *Wave 1*. The absorbed power trends provided by the standard MPC, augmented MPC and the MPC with known disturbance are illustrated by the blue, red and green line respectively.

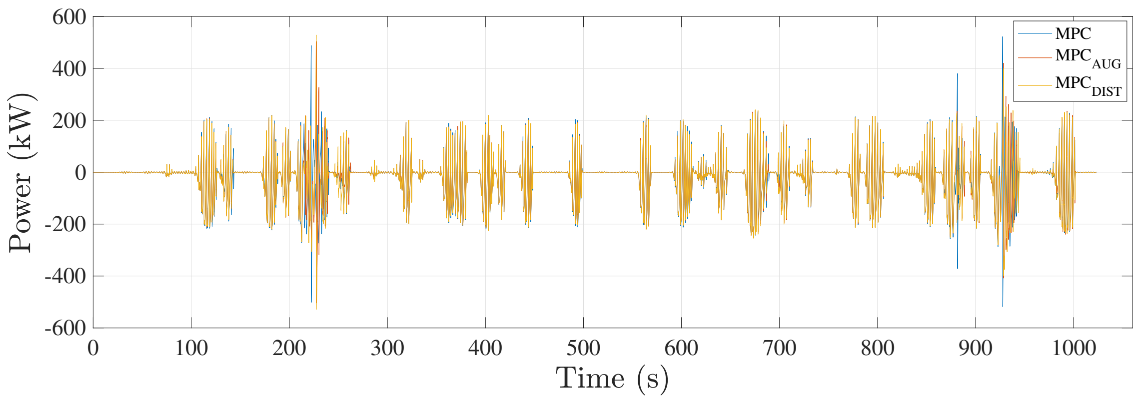

Figure 3.31: Absorbed Power Plot - MPC vs Augmented MPC vs MPC with Known Disturbance ($H_p = 20$)

The figure 3.32 shows a section of the previous figure 3.31 which shows the different absorbed power capabilities by the three different MPC approaches when the prediction horizon is to $H_p = 20$.

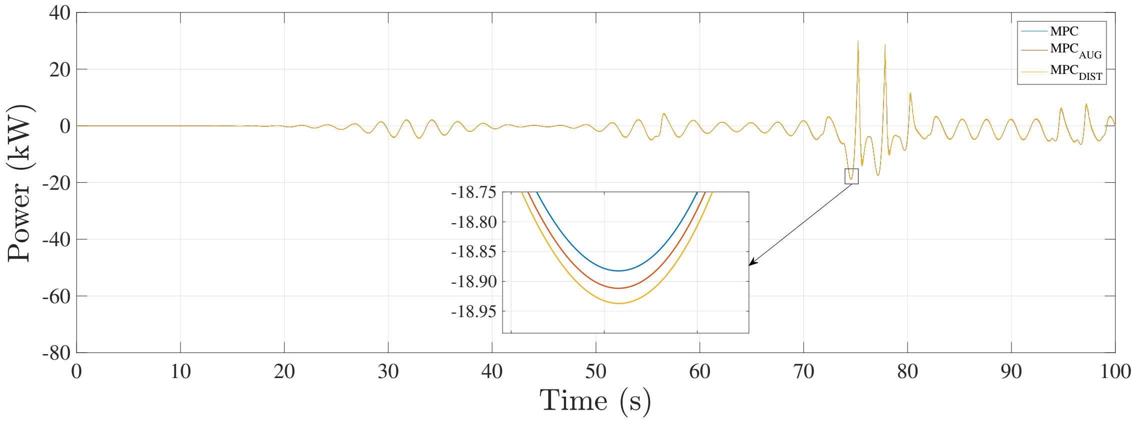

Figure 3.32: Absorbed Power Plot (section) - MPC vs Augmented MPC vs MPC with Known Disturbance ($H_p = 20$)

From figure 3.32 it is thus possible to observe that the *MPC with known disturbance* is able to extract more power than the other two MPC approaches, provided that the prediction horizon is long enough to make differences with respect to the *augmented MPC* approach.

Chapter 4

LQR Control for ISWEC

A further investigation about the maximization of the produced power has been done evaluating the results provided by the *LQR control* approach. This control technique results in a *static state feedback control law*, which thus results in a much simpler implementation from the computational effort point of view. The next subsections will introduce the main theory concepts about the LQR technique and will discuss its usage for controlling the ISWEC system as well as the obtained results.

4.1 Introduction to LQR Theory

LQR stands for *Linear Quadratic Regulator* and it is control technique based on the *optimal control* approach, and it is implemented through a static state feedback architecture. As well as MPC technique also LQR makes use of a *cost function*, which is tuned to obtain the best tradeoff among the system requirements.
Despite based on the same principle, the LQR control implementation is much simpler than the MPC technique, and for this reason it does not include the possibility to take into account constraints of the system in the control problem.

More in the details, the LQR control addressed for the ISWEC system is referred to as *infinite-horizon discrete-time LQR*, and it is defined as follows:

$$\min_{U(k)} J\big(\boldsymbol{x}(k), U(k)\big) = \min_{U(k)} \sum_{i=0}^{\infty} \boldsymbol{x}^T(k+i)\,\boldsymbol{Q}\,\boldsymbol{x}(k+i) + u^T(k+i)\,\boldsymbol{R}\,u(k+i) \tag{4.1}$$

Subject To:

$$\boldsymbol{x}(k+1) = \boldsymbol{A}\,\boldsymbol{x}(k) + \boldsymbol{B}\,u(k)$$

Where $U(k)$ is the vector containing the sequence of all the command actions $u(k)$, from k to the *prediction horizon* H_p, that in this contexts is set as $H_p = \infty$.

$$U(k) = \big[u(k), \quad u(k+1), \quad u(k+2), \quad \ldots\big] \tag{4.2}$$

The matrices $\boldsymbol{Q}$ and $\boldsymbol{R}$ are design parameters and have to satisfy the following conditions:

- $\boldsymbol{Q} = \boldsymbol{Q}^T \succeq 0\,, \quad \boldsymbol{Q} \in \mathbb{R}^{n \times n}$
- $\boldsymbol{R} = \boldsymbol{R}^T \succ 0\,, \quad \boldsymbol{R} \in \mathbb{R}^{n_u \times n_u}$

with n the system order and n_u the input order.

$J\big(\boldsymbol{x}(k), U(k)\big)$ is the *cost function* and as for the MPC technique it depends both on the current state $\boldsymbol{x}(k)$ and on the sequence command actions $U(k)$, as shown in (4.2).

If the matrices $\boldsymbol{A}$ and $\boldsymbol{B}$ are reachable it's possible to show [16] that the *infinite-horizon discrete-time LQR* problem (4.1) can be solved and the solution consists in the *optimal* command action referred to as $u^*(k)$ and is implemented through a *static state-feedback control law* defined as:

$$u^*(k) = -\boldsymbol{K}\, x(k) \tag{4.3}$$

with:

$$\boldsymbol{K} = (\boldsymbol{R} + \boldsymbol{B}^T \boldsymbol{P}\, \boldsymbol{B})^{-1} \boldsymbol{B}^T \boldsymbol{P}\, \boldsymbol{A}$$

where $\boldsymbol{P}$ is shown to exist and to be a *constant symmetric positive definite matrix* $\boldsymbol{P} = \boldsymbol{P}^T \succ 0$, and is computed as the solution the *Discrete-time Algebraic Riccati Equation (DARE)*:

$$\boldsymbol{P} = \boldsymbol{A}^T \boldsymbol{P}\, \boldsymbol{A} + \boldsymbol{Q} - \boldsymbol{A}^T \boldsymbol{P}\, \boldsymbol{B}\, (\boldsymbol{R} + \boldsymbol{B}^T \boldsymbol{P}\, \boldsymbol{B})^{-1} \boldsymbol{B}^T \boldsymbol{P}\, \boldsymbol{A}$$

About stability properties of the feedback control system whose controller is the discussed LQR it is possible to show that:
"Assuming that the matrices $\boldsymbol{A}$ and $\boldsymbol{B}$ are both reachable and the matrices $\boldsymbol{A}$ and $\boldsymbol{Q}^{\frac{1}{2}}$ are both observable, then the closed-loop system described by the state equation $\boldsymbol{x}(k+1) = (\boldsymbol{A} - \boldsymbol{B}\,\boldsymbol{K})\,\boldsymbol{x}(k)$ is asympotically stable".

4.2 Control System Architecture

The feedback control system architecture is reported in figure 4.1. The architecture corresponds to the one characterizing the *standard MPC*, where the only difference lies in the implemented controller which in this case is based on the LQR technique. Therefore, the induced torque by the wave τ_w excites the ISWEC system while the LQR controller measures the system states and accordingly computes the command action T_ε which drives the PTO unit.

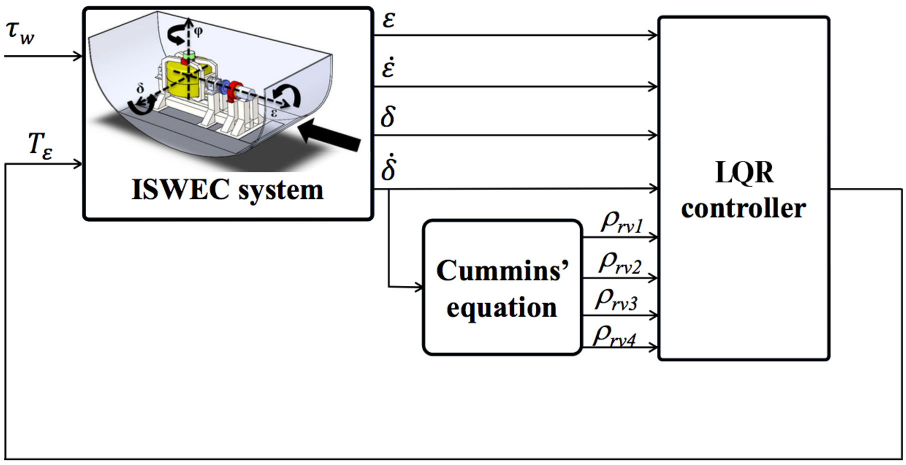

Figure 4.1: Control System Architecture - LQR

The Simulink model implementing the introduced architecture is illustrated in figure 4.3, which as for the architecture it corresponds to the *standard MPC* model with the exception of the implemented controller which in this case is an LQR. The *CONTROLLER* subsystem takes in input the measurable *states* which are $\dot{\varepsilon}(k)$, $\varepsilon(k)$, $\dot{\delta}(k)$ and $\delta(k)$, and provides the command action $T_\varepsilon(k)$ as output.
As for the *MPC* model the *CONTROLLER* subsystem contains besides the *LQR controller* also the *Full State Builder* subsystem intended for providing the 4 hydrodynamic states $\rho_{rv,1}(k)$, $\rho_{rv,2}(k)$, $\rho_{rv,3}(k)$ and $\rho_{rv,4}(k)$ computed basing on the measure of the state $\dot{\delta}(k)$.

In figure 4.3 it is possible to see the implementation of the LQR controller. This results in a matrix multiplication of the measured state $\boldsymbol{x}(k)$ by the matrix $\boldsymbol{K}$, seen in equation (4.3). Moreover, the LQR technique does not allow for taking into account the constraints of the system in the control problem, therefore a saturation of the command action is required to avoid large command torques that the PTO electric motor is not able to exert.

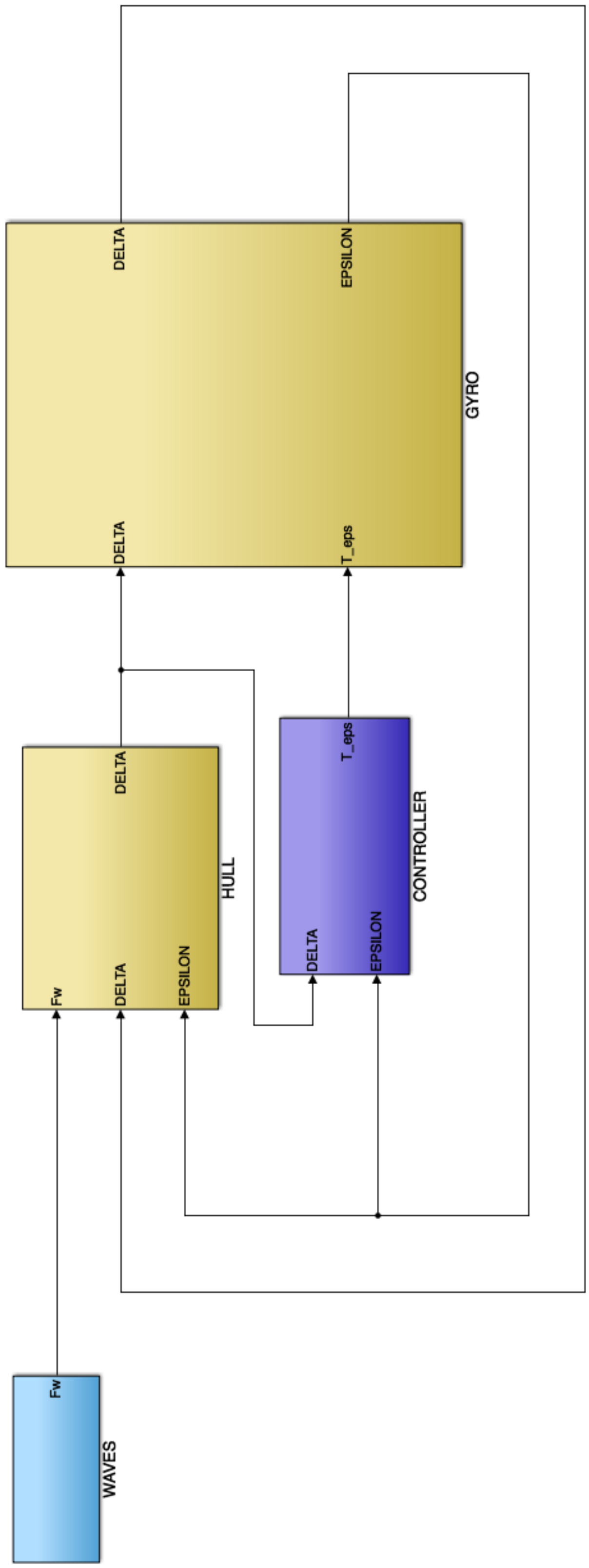

Figure 4.2: Simulink Model - LQR

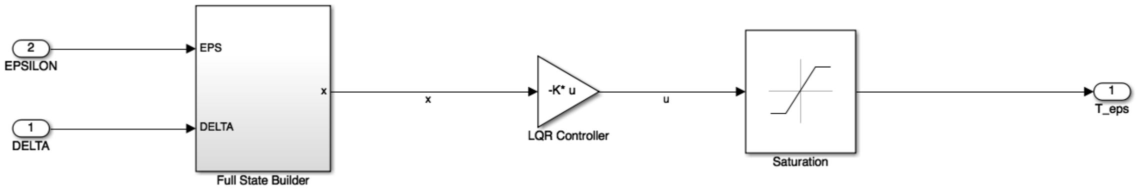

Figure 4.3: Controller Subsystem - LQR

4.3 LQR Control Problem

The LQR control problem is slightly more complex in the ISWEC context with respect to the definition shown in (4.1) presented in the *LQR theory* section, since in this case the *cost function* has to be customized in order to include the mixed term related to the power absorption. The mixed term involves at the same time both the PTO shaft angular speed $\dot{\varepsilon}(k)$ and the command action $T_\varepsilon(k)$, as explained in the *standard MPC* context.

The ISWEC model used for control purposes is the linearized model also used for *standard MPC* explained in subsection 3.2.2, hereafter reported.

$$\boldsymbol{x}(k+1) = \boldsymbol{A}_{DT}\,\boldsymbol{x}(k) + \boldsymbol{B}_{DT}\,u(k) \tag{4.4}$$

The sampling time T_s used for discretizing the *continuous-time model* is chosen as 50 ms as well as for the *MPC* control problem.

It is possible to see that also for the LQR case the ISWEC model does not take into account the contribution of the incoming induced torque by the wave in the system dynamics. As well as for MPC context also in LQR control problem the *cost function* is defined as:

$$J(k) = \sum_{k=1}^{H_p-1} q_{11}\,\dot{\varepsilon}(k)^2 + q_{22}\,\varepsilon(k)^2 + 2\,n_1\,\dot{\varepsilon}(k)\,T_{PTO}(k) + r\,T_{PTO}(k)^2 \tag{4.5}$$

which comes from the standard compact form:

$$J(k) = \sum_{k=1}^{H_p-1} \begin{bmatrix} \boldsymbol{x}(k)^T & u(k) \end{bmatrix} \begin{bmatrix} \boldsymbol{Q} & \boldsymbol{N} \\ \boldsymbol{N}^T & \boldsymbol{R} \end{bmatrix} \begin{bmatrix} \boldsymbol{x}(k) \\ u(k) \end{bmatrix} \tag{4.6}$$

where:

$$\boldsymbol{Q} = \begin{bmatrix} q_{11} & 0 & 0 & \dots & 0 \\ 0 & q_{22} & 0 & \dots & 0 \\ 0 & 0 & 0 & \dots & 0 \\ \vdots & \vdots & \vdots & \ddots & \vdots \\ 0 & 0 & 0 & \dots & 0 \end{bmatrix} \in \mathbb{R}^{8\times 8}, \quad \boldsymbol{N} = \begin{bmatrix} n_1 \\ 0 \\ 0 \\ \vdots \\ 0 \end{bmatrix} \in \mathbb{R}^{8\times 1}, \quad \boldsymbol{R} = r \in \mathbb{R} \tag{4.7}$$

The terms of the *cost function* 4.5 have the same meaning already discussed for the MPC control problem in subsection 3.2.2, with the difference that the weights are tuned according to a different criteria, as explained in the next subsection.

4.4 Implementation

The implementation of the LQR controller takes place entirely in MATLAB and Simulink, without the usage of any toolbox. The procedure followed to design the LQR is hereafter enumerated.

LQR control problem implementation:

I) Definition and tuning of the matrices $\boldsymbol{Q}$, $\boldsymbol{R}$, $\boldsymbol{N}$;

II) Computation of the gain matrix $\boldsymbol{K}$ by means of the MATLAB native command
`>> lqr(sys,Q,R,N);`

III) Deployment of the computed gain matrix $\boldsymbol{K}$ in the Simulink feedback control system.

Where `sys` in the LQR command is a variable containing the description of the linearized ISWEC system, whereas `Q,R,N` are the weight matrices $\boldsymbol{Q}$, $\boldsymbol{R}$, and $\boldsymbol{N}$ defined in (4.7) whose entries are defined as follows [9]:

$$q_{11} = \frac{T_{max}}{\dot{\varepsilon}^2_{max}}$$

Where T_{max} and $\dot{\varepsilon}_{max}$ are respectively the maximum feasible PTO torque and the maximum angular speed of the PTO shaft.

$$q_{22} = \frac{T_{max}}{\varepsilon^2_{max}}$$

Where ε_{max} is the maximum angle that the PTO shaft is allowed to achieve, and has been chosen as 2π.

$$r \ll \frac{1}{T_{max}}\,, \quad n_1 = \frac{1}{2\,\dot{\varepsilon}_{max}}$$

The introduced definitions of the LQR parameters result in the numerical values summarized in table 4.1.

Table 4.1: LQR Parameters

Parameter	**Value**	**Description**
T_s	50 (ms)	Sampling Time
q_{11}	6250	Q matrix weight
q_{22}	2533	Q matrix weight
r	$1 \cdot 10^{-7}$	R matrix Weight
n_1	0.125	N matrix weight

4.5 Results

The results provided by the LQR technique are obtained through simulations of the nonlinear ISWEC model shown in figure 4.3 and are evaluated through MATLAB data and plots.

The figure 4.4 shows the the absorbed power trend when the system is excited by the wave profile classified *Wave 1* comparing the LQR illustrated by the green line with the MPC result illustrated by the red line.

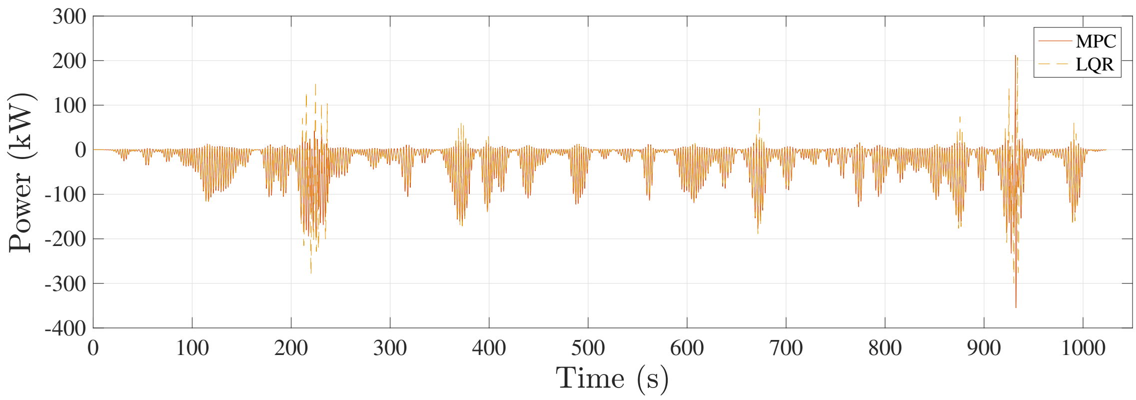

Figure 4.4: Absorbed Power Plot - LQR vs MPC

From this figure it is possible to understand that the two power trends are quite different despite similar, but for a clearer evaluation it is possible to observe the figure 4.5 which represents a section of the plot in which it is also shown a magnified portion containing a peak value.

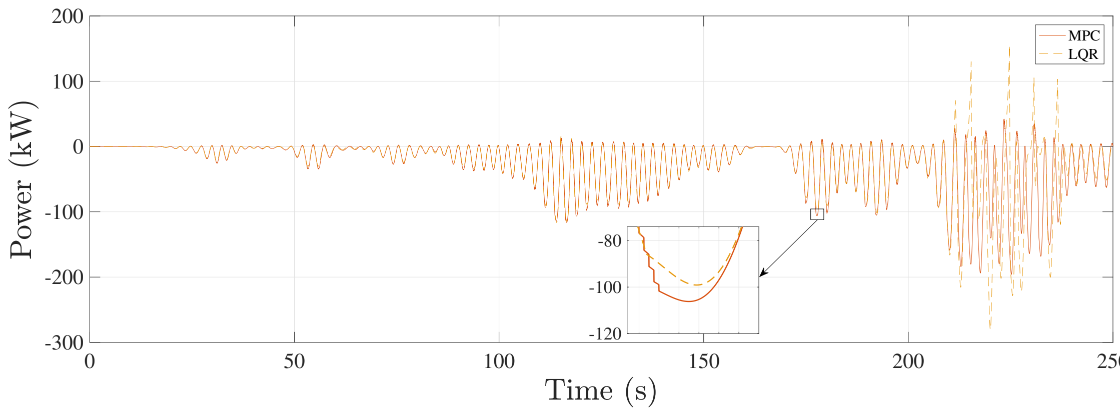

Figure 4.5: Absorbed Power Plot (section) - LQR vs MPC

From figure 4.5 it is possible to see that the LQR control imitates quite well the MPC control approach, but with some crucial differences. In particular:

- It is possible to observe that in nominal conditions, represented by the plot form 0 s to about 200 s, the MPC control allows to harvest an higher quantity of power than the LQR technique as the its negative peaks results in general greater;
- The cases in which the excitation wave becomes rougher, that in the presented plot occurs after 200 s (see figure 3.5), the LQR control is not able keep the absorbed power trend to negative quantities. This observable from the positive peaks characterizing the LQR absorbed power trend after 200 s. This results in a actual absorbed power, differently from the MPC control which instead, as already seen, shows the capability of keeping the absorbed power trend almost always negative for all its course.

For a quantitative analysis it is possible to evaluate the *produced mean power* defined as

$$\overline{P} = -\frac{1}{n_s}\sum_{k=1}^{n_s} P(k)$$

Given the *produced mean power* $\overline{P}$ values for the nine wave profiles provided by the *LQR* control it is possible to compute the *normalized produced mean power* as

$$\widehat{P} = \frac{\overline{P}}{\overline{P}_{max}}$$

where $\overline{P}_{max}$ is the maximum produced mean power among the *PD*, *LQR* and *MPC* provided results for the nine wave profiles.

The table 4.2 summarizes the the *normalized produced mean power* for the nine sea states of interest (reported in table 3.2) obtained from PD, MPC and LQR respectively referred to as $\widehat{P}_{PD}$, $\widehat{P}_{LQR}$ and $\widehat{P}_{MPC}$.

Table 4.2: Normalized Produced Mean Power - LQR

Wave ID	$\widehat{P}_{PD}$	$\widehat{P}_{LQR}$	$\widehat{P}_{MPC}$
1	0.3647	0.4041	0.4149
2	1.00	0.9157	0.9787
3	0.0125	0.0499	0.0552
4	0.0232	0.0721	0.0794
5	0.2385	0.2907	0.3037
6	0.2844	0.3457	0.3669
7	0.063	0.1427	0.1635
8	0.5058	0.5399	0.5614
9	0.0696	0.1202	0.1241

From table 4.2 it is possible to observe that the *produced mean power* obtained through LQR technique generally places between the PD and the MPC results, with the only exception of the sea state defined by *Wave 2*, where the PD control provides a slightly greater produced power than both LQR and MPC control approaches.

It is possible to analyse the produced mean power percentage increment provided by the LQR control for the nine wave profiles of interest according to

$$\Delta\overline{P}_{LQR} = \frac{\overline{P}_{LQR} - \overline{P}_{PD}}{\overline{P}_{PD}}$$

whose results are reported in the following table 4.3 together with the percentage increment provided by the standard MPC approach already reported in table 3.4.

Table 4.3: Produced Power percentage increment - LQR

Wave ID	$\Delta\overline{P}_{LQR}$ (%)	$\Delta\overline{P}_{MPC}$ (%)
1	+ 10.83	+ 13.79
2	− 8.41	− 2.13
3	+ 296.77	+ 337.27
4	+ 211.25	+ 242.33
5	+ 21.90	+ 27.32
6	+ 21.00	+ 28.99
7	+ 126.74	+ 159.68
8	+ 6.76	+ 10.97
9	+ 72.89	+ 78.34

According to the sea states occurrences defined in table 3.2 it is possible to evaluate the yearly energy production E_{year}^{LQR} provided by the LQR technique according to the formula defined in (3.17).
The table 4.4 reports the *normalized yearly energy production* provided by the PD and the MPC approach.

Table 4.4: Normalized Yearly Energy Production - LQR

$\widehat{E}_{year}^{PD}$	$\widehat{E}_{year}^{LQR}$	$\widehat{E}_{year}^{MPC}$
0.8432	0.948	1.00

The results reported in table 4.4 show how the LQR technique is able to provide an higher yearly energy production but still lower than the more advanced MPC technique is able to harvest.

It is possible to evaluate the percentage increment of the yearly energy production provided by the LQR control with respect to the previous developed PD control by evaluating

$$\Delta E_{year}^{LQR} = \frac{E_{year}^{LQR} - E_{year}^{PD}}{E_{year}^{PD}}$$

which gives

$$\Delta E_{year}^{LQR} = 12.43\,\%$$

The table 4.5 summarizes the percentage increment of the yearly energy production provided by both LQR and MPC with respect to the PD control, respectively referred to as ΔE_{year}^{LQR} and ΔE_{year}^{MPC}.

Table 4.5: Yearly Energy Production percentage increment - LQR vs MPC

ΔE_{year}^{LQR} (%)	ΔE_{year}^{MPC} (%)
12.43	18.59

From the analysis of table 4.5 it is possible to conclude that the LQR is a valid technique which allows to produce an yearly energy greater than PD controller. The MPC control nevertheless is able to provide a significantly higher yearly produced energy with respect to the LQR, with the cost of a more complex control implementation and thus with the requirement of a suitable processor platform able to achieve the required computational effort.

Chapter 5

Conclusions

This thesis has shown the effectiveness of the *Model Predictive Control* (MPC) technique for controlling the *Inertial Sea Wave Energy Converter* (ISWEC) aiming to maximize the production of the electric power.

In particular, an original *Model Predictive Control* has been presented, which proposes a predictive control formulation that effectively handles the performance tradeoff among different control objectives such as power production, control effort minimization, gyroscope shaft speed limitation and position stabilization. Moreover, system constraints have been accounted for and fulfilled as well.

Significant performance improvements have been obtained with respect to previous available proportional-derivative (PD) control, in terms of energy production, requested torque energy and gyroscope shaft speed limitation.

A linear model of the considered wave energy converter device is employed to cast the underlying optimization problem as a quadratic programme to obtain a fast online implementation of the controller on a commercial processor control unit platform by means of an efficient solver. Furthermore, the adopted sampling time result to be quite long such to be suitable for the implementation on not expensive processor units. Extensive simulations performed on a detailed nonlinear model of the wave energy converter have shown the effectiveness of the introduced approach.

Furthermore, it has been designed an *augmented MPC* controller capable of taking into account the wave contribution in the dynamics prediction in an approximated form, and it has been proven to provide improved results despite in a slight extent with respect to the *standard MPC*.

Moreover, the *MPC with known disturbance* has been designed, characterized to be capable of considering the real wave contribution into the dynamics prediction, and it has been proven not to provide significant improvements with respect to the *augmented MPC* according to the optimal tuning suited for the ISWEC requirements.

Finally, the *Linear Quadratic Regulator* (LQR) control has been investigated as well in order to analyse the achievable performances through a simpler controller still based on optimal control. The LQR control approach has shown improved results with respect to the PD control despite lower than the MPC approach ones. Nevertheless the LQR technique may result a suitable choice in case of a processor platform with low computational capabilities is required to be used.

Future Developments

Starting form the designed MPC controller it is possible to carry out further developments.

A first development which can be investigated is the hardware implementation of the proposed MPC controller. In particular it is possible to implement the quadratic programme algorithm together with the receding horizon principle technique generating a suitable code in order to be deployed on an hardware device. It is therefore possible to make experimental validations by comparing the simulation results with the measured quantities from the hardware device.

Another possible development may consist in designing an MPC controller based on a more sophisticated ISWEC model. In particular the MPC controller designed in this thesis has adopted a linearized model of the ISWEC system characterized by 2 DoF, but also a 3 DoF ISWEC model is available which has been proven to provide slightly more accurate results. It is thus possible to design an MPC controller based on this 3 DoF model and to test its effectiveness by means of the productivity evaluation procedure presented in this thesis work.

Bibliography

[1] D. Magagna and A. Uihlein, "Ocean energy development in europe: Current status and future perspectives," *International Journal of Marine Energy*, vol. 11, pp. 84–104, 2015. [Online]. Available: http://www.sciencedirect.com/science/article/pii/S2214166915000181.

[2] J. V. Ringwood, G. Bacelli and F. Fusco, "Energy-maximizing control of wave-energy converters," *IEEE Control Systems Magazine*, vol. 34, no. 5, pp. 30–55, 2014.

[3] T. Aderinto and H. Li, "Ocean wave energy converters: Status and challenges," *Energies*, vol. 11, p. 1250, 05 2018.

[4] S. Salter, "The use of gyros as a reference frame in wave energy converters," *Proceedings of the 2nd International Symposium on Wave Energy utilization*, pp. 99–115, 06 1982.

[5] F. Salcedo, P. R. Minguela, R. R. Arias, P. Ricci, and M. Santos-Mugica, "Oceantec: Sea trials of a quarter scale prototype," 01 2009.

[6] H. Kanki, S. A. ans T. Furusawa, and T. Otoyo, "Development of advanced wave power generation system by applying gyroscopic moment," 7 2009, pp. 280–283.

[7] G. Bracco, E. Giorcelli, and G. Mattiazzo, "Iswec: A gyroscopic mechanism for wave power exploitation," Mechanism and Machine Theory, vol. 46, no. 10, pp. 1411–1424, 2011, cited By 41.

[8] M. Raffero, M. Martini, B. Passione, G. Mattiazzo, E. Giorcelli, and G. Bracco, "Stochastic control of inertial sea wave energy converter," *The Scientific World Journal*, vol. 2015, pp. 1–14, 2015.

[9] G. Vissio, D. Valério, G. Bracco, P. Beirao, N. Pozzi, and G. Mattiazzo, "Iswec linear quadratic regulator oscillating control," *Renewable Energy*, vol. 103, pp. 372–382, 2017.

[10] G. Bracco, E. Giorcelli, G. Mattiazzo, B. Passione, E. Prudentino, M. Raffero, and G. Vissio, "Application of linear model predictive control to the iswec," in *Renewable Energies, C. Guedes Soares (Ed.)*, 2015, pp. 257–264.

[11] G. Bracco, A. Cagninei, E. Giorcelli, G. Mattiazzo, D. Poggi, and M. Raffero, "Experimental validation of the iswec wave to pto model," *Ocean Engineering*, vol. 120, pp. 40–51, 2016.

[12] W. E. Cummins, “The impulse response function and ship motions,” *Schiffstechnik*, vol. 9, pp. 101-109, 1982.

[13] T. Pérez and T. Fossen, “Time- vs. frequency-domain identification of parametric radiation force models for marine structures at zero speed,” *Modeling, Identification and Control*, vol. 29, no. 1, pp. 1–19, 2008.

[14] E. Prudentino, “A model based control strategy,” *MSc Thesis, Politecnico di Torino*, 2014.

[15] G. Vissio, “ISWEC toward the sea Development, Optimization and Testing of the Device Control Architecture,” *PhD Dissertation, Politecnico di Torino*, 2017.

[16] B. D. O. Anderson, J. B. Moore, “Optimal Control - Linear Quadratic Methods,” *Prentice Hall*, 1989.